ESTIMATING BSPS USING MRI, DPX, AND PHOTOGRAMMETRY

DEVELOPING A METHOD FOR ESTIMATING BODY SEGMENT PARAMETERS USING DUAL PHOTON ABSORPTIOMETRY, MAGNETIC RESONANCE IMAGING, AND PHOTOGRAMMETRY

By

MAT MERCURI, B.KIN.

A Thesis

Submitted to the School of Graduate Studies

in Partial Fulfilment of the Requirments

for the Degree

Master of Science

McMaster University

MASTER OF SCIENCE (2004) McMaster University
(Human Biodynamics) Hamilton, Ontario

TITLE: Developing a method for estimating Body Segment Parameters using Dual Photon Absorptiometry, Magnetic Resonance Imaging, and Photogrammetry

AUTHOR: Mat Mercuri, B.Kin. (McMaster University)

SUPERVISOR: Dr. J.J. Dowling

NUMBER OF PAGES: ix, 78

Abstract

An accurate estimation of Body Segment Parameters (BSPs) is needed to understand human movement. These include segment mass, centre of mass, and moment of inertia about the centre of mass. Bone density scanners, such as DPX, can measure BSPs, but are limited to only two dimensions. MRI produces images in three dimensions, but cannot directly measure mass. For this study, MRI was used in conjunction with a DPX scan of the human body. The result was the development of a method to estimate mass, and subsequently, centre of mass, and moment of inertia from MRI images. Next, ellipses were created from the dimensions of transverse plane slices (produced from MRI). Three different density profiles were applied to the ellipses, and mass, centre of mass and moment of inertia about the centre of mass of each slice was calculated. It was found that constant density transverse plane ellipses could be used to estimate BSPs for most regions of the body. Photogrammetry can also be used to generate the dimensions of ellipses that represent transverse plane slices. Therefore, the suitability of photogrammetry to estimate slice BSPs was tested. It was found that depending on the density profile used, photogrammetry is an effective method for estimating BSPs. An exception to this estimation was in the chest, where ellipses may not be representative of the body.

Acknowledgments

I would like to thank my advisor, Dr. James J. Dowling for his supervision and support during the course of my education, both undergraduate and graduate. As well, a special thanks goes out to Marc Klimstra, and Dr. Jennifer Durkin for their friendship and counsel(ing), especially over the past two years. I am forever grateful.

Thanks to Dr. Gail Frost, and Dr. Michael Pierrynowski for being on my supervisory committee, and to Leigh Marshall for your help on the project.

My family deserves my appreciation for supporting me all these years. Everything you have done to help was... well... helpful. To my friends: especially Joe, Steph and Chloe, Tim Knapp, Kristina Kolezar, and Peter Merriman (I can include my brother Johnny Mercuri here as well)... thanks for being.

Finally, I would like to thank my grandmother, Mary Mercuri, who passed away last summer. Thank you for your unconditional love and support over the years. You were and are still an inspiration to all those who had the fortune of knowing you.

If I could do just one near perfect thing I'd be happy,
They'd write it on my grave, or when they scattered
my ashes
On second thoughts I'd rather hang around and be there
with my best friend,
If she wants me.
-Belle and Sebastian

Table of Contents

List of Figures

Study 1

Study 2

Study 3

Introduction

An understanding of human anthropometrics is important in to understand human motion. Hinrichs (1985) once noted that a lack of understanding body segment parameters (BSPs), such as segment mass, centre of mass, and moment of inertia, is the greatest source of error in biomechanics research. It is important to have accurate measures of these, since some BSPs and inertial characteristics are dependent on others. For example, the calculation of mass may be dependent on segment density and volume. An error in measuring any of these may then translate into an error in calculating the moment of inertia for a segment.

BSPs are also used with kinematic measures to calculate kinetic variables such as muscle moment and force about and at a joint. Often, biomechanists take an inverse dynamics approach to calculate the internal kinetics or a forward dynamics approach to determine the kinematics of the body. These methods require the body to be treated as a chain of rigid links connected with frictionless joints (Winter, 1990). The scientist will take kinematic measures at the extremities and work inward, thus calculating forces based on the previous limb's kinetic and kinematic values. If the BSP calculations are incorrect for a limb, errors in kinetic calculations will result. This error may not be large at first, but compounding it with other calculations based on incorrect BSPs can cause an exaggeration of the error after a few iterations. Therefore, in order to reduce such problems, anthropometrics has been an important area of biomechanical research over the past century and a half.

Cadaver Studies

While many of the post-Renaissance scientists examined the structure of the human body as a mechanical system, it wasn't until the late 19th Century that anthropometry research became comprehensive. At this point cadaver studies were fashionable, and it was Harless (1860) who was the first to report an analysis of BSPs. Harless did an extensive analysis of two dissected cadavers. The cadavers were cut through the joint centres. Body segment parameters were then directly measured, or calculated based on measurements of the cadavers. Mass and centre of gravity were calculated using the balance method. That is, the segment is placed on a knife edge, with the centre of mass being the location that allows the segment to be balanced (i.e. the segment does not wobble or fall off the knife) (Drillis and Contini, 1966; Pearsall and Reid, 1994). The 19th Century saw another widely reported cadaver study - this by Braune and Fischer (1889). Braune and Fischer determined both the lengths and masses of individual segments by studying three male cadavers. Drillis and Contini later used this cadaver data to develop regression equations that predict body segment parameters (Drillis and Contini, 1966).

Among the cadaver studies to date, one of the most extensive, and widely was performed by Dempster (1955). While at Wright-Patterson Air Force Base, Dempster did

an examination of eight male specimens, aged 52 to 83. The BSPs Dempster measured were segment mass, density, centre of mass, and moment of inertia (Pearsall and Reid, 1994). The knife-edge balance technique was used to estimate the location of the centre of mass. Mass was measured by weighing the individual segments. In combination with the parallel axis theorem, the pendulum technique was used to calculate the moments of inertia for each segment. As with the Braune and Fischer data, Drillis and Contini (1966) used the data collected from this experiment to create regression equations that predict the aforementioned body segment parameters.

Clauser, McConville and Young (1969) performed the last of the classic cadaver studies. Clauser et al. used thirteen male cadavers, aged 24 to 78, to calculate segment volume, density, mass, centre of mass, and moment of inertia. Centre of mass was calculated using the knife edge balance method (as per Harless), while volume was calculated by water immersion. Clauser et al. then developed regression equations in order to predict body segment parameters for the entire human population (Clauser, McConville and Young, 1969).

Cadaver studies are important in the history of understanding BSPs for the human body in that the researchers mentioned above identified which parameters are important for analyzing human movement. Also, the trailblazers of anthropometry research should be respected in their clever approaches to measuring BSPs. Unfortunately, cadaver studies do not fully depict the true nature of human BSPs, and while cadaver research allowed for their examination, more work needed to be done.

Specifically, cadaver research was flawed in that each study had very few subjects, the majority of these subjects were elderly Caucasian males, and therefore, the regression equations developed from these cadaver data cannot be generalized for a larger population. Thus, it is believed that these equations cannot be used to predict the body segment parameters of a diverse population without a great deal of error.

In retrospect, cadaver studies are problematic from the point of view of a contemporary scientist in that each study used different segmentation techniques. Discrepancy between segmentation methods limits the ability to compare data, and thus, predictive equations (Durkin, 1998). As well, with the segmentation of cadavers, fluid and tissue is lost. This loss of fluid and tissue decreases the true mass of the segment, which can cause an underestimation of the mass and moment of inertia (which is dependent on mass and its distribution) when regression equations are developed.

Living Subject Studies

The limitations recognized in the cadaver studies prompted a move towards the development of techniques that can estimate BSPs in living subjects. Such techniques include water immersion, photogrammetry, and medical imaging, such as magnetic resonance and computed tomography. Data collected using these techniques were then

used to create mathematical models (including regression equations and geometric models) that can accurately represent the inertial characteristics of an individual or a population.

Water Immersion

The precursor to the water immersion technique was water displacement. Based on these principles, researchers such as Spivak (1915), and Zook (1932) used water displacement to estimate whole body volume. The water immersion technique is based on the principle that the volume of water displaced is equal to the volume of the object submerged. Density estimates can be made for a body completely submerged based on Archimedes' principle for buoyant forces. In an early study devised by Drillis and Contini (1966), measurements of each segment's length, volume, density, mass, centre of mass, and moment of inertia were made from twelve living male subjects aged 20 to 39. Volume and density measures were made through the water immersion technique. Moment of inertia was calculated using the pendulum swing method (Drillis and Contini, 1966; Pearsall and Reid, 1994). The pendulum method calculates moment of inertia about an axis based on the oscillation period of a segment swinging about that axis.

In his 1983 work, Plagenhoef compared the BSP estimates of 100 young females and 35 males with those estimated by Dempster (1955). Segment volume, mass and centre of mass were calculated for each subject. Water immersion was used to calculate volume (Pearsall and Reid, 1994). As well, Plagenhoef constructed lead models from plaster models of subject limbs. These lead models were used to measure the radius of gyration for each segment (Plagenhoef, 1983).

Water immersion is problematic in estimating BSPs because of one of its assumptions. That is, in order to calculate segment mass, water immersion must assume a uniform density of known value throughout each segment immersed. Often, the density values used were based on cadaver research. As noted earlier, cadavers may not retain the physical properties of living subjects.

Photogrammetry

While water immersion allowed for an accurate estimate of segment volume, the technique does not describe shape. Shape may be important because moment of inertia measures for a segment are dependent on mass distribution. This led to the need for a technique that allowed for an accurate estimation of segment volume, while keeping the distribution of the segment volume (and thus mass and moment of inertia measures) faithful. Photogrammetry, a technique promoted by Jensen (1978), measures the shape of an object from two or more pictures of that object. Photographs in the frontal and sagittal plane allow for a measurement of a segment's length, width, and depth. These measurements are then used as the dimensions of a three dimensional ellipse, in which

the volume and centre of mass of the segment can be estimated. Multiplying this volume by a density allows for an estimation of mass, and subsequently, moment of inertia.

The first widely reported study to use photogrammetry was performed by Wild (1954). Later Drillis and Contini used photogrammetry to estimate limb segments paramters (Drillis and Contini, 1966). Chandler (1978) used the technique in order to estimate volume, mass, centre of mass, and moment of inertia for the body segments of 37 children, both male and female. Jensen also used photogrammetry to measure BSPs in children; this study addressed the need to discriminate between body types (Jensen, 1978). These studies demonstrated photogrammetry as a practical method for providing investigators with a means of gathering data on large samples of living subjects.

Jensen's work points out differences within a population, such as changes in body shape as people age (Jensen, 1989; Jensen and Abraham, 1990; Jensen and Fletcher, 1994). When compared to early studies on children, these studies have provided insight into BSP diversity for different population groups, such as the difference between adults and children, males and females, etc. (Pearsall and Reid, 1994).

Having recognized population shape differences, Jensen (Jensen, 1989; Jensen and Abraham, 1990; Jensen and Fletcher, 1994) proceeded to demonstrate the need for a thorough understanding of segment density. Many anthropometric models assume a uniform density throughout each segment. Jensen examined how density changes throughout a segment, and advocated the application of density profiles to anthropometric models (Wei and Jensen, 1995). For example, because the ratio of bone tissue to lean and fat tissue changes throughout the segment, the density of the forearm segment is higher at both the proximal and distal ends. Jensen has shown that such a difference can have adverse effects on the accurate measurement of some BSPs such as moment of inertia in each of the three major axes. That is, the difference between using a constant segment density and a density profile that accounts for changes through a segment averaged 3.8%, but ranged up to 22.5% when estimating moment of inertia for individual segments (Wei and Jensen, 1995).

While photogrammetry studies allowed for the accumulation of large data samples on a wide variety of subpopulations, the uniform density assumption needs to be addressed in further detail before mass, and thus inertial characteristics dependent on mass, can be accurately measured for body segments. If density issues can be solved, photogrammetry may become a quick, cheap and accurate method of determining the BSPs for an individual. As well, when applied to a larger population, perhaps regression equations or geometric models may be developed to represent human subpopulations (age, gender, and culture).

Medical Imaging

As technology advances, researchers are provided with the means for a novel approach to study design. The onset of new medical imaging technologies, such as gamma-ray scanners, computed tomography (CT) and magnetic resonance imaging (MRI), have allowed for advances in BSP estimation, especially on living subjects. Zatsiorsky and Seluyanov (1983; 1985) were among the first to advocate the use of imaging technology as a tool for anthropometry research. With the use of gamma-ray scanning technology, Zatsiorsky and Seluyanov (1983) assessed 100 males in order to estimate segment lengths, masses, centres of mass, and moments of inertia. Regression equations were then developed in order to predict the anthropometrics and inertial characteristics of a number of segments for the human population.

Huang first used CT as a means for measuring human tissue densities (Huang and Wu, 1976). This study showed that computed tomography directly measures tissue density within a defined space and volume of a segment. Once tissue densities are defined, BSPs can then be reconstructed. Having established tissue densities, Huang (1983) used CT to compare the body segment parameters of a human cadaver with those of a pig specimen.

The next step was to use computed tomography on a number of living subjects in order estimate human anthropometrics and inertial characteristics. The first widely reported such study was by Zheng et al. (1990), who used CT on fifteen males and four females to estimate the inertial characteristics of each segment. Recognizing some of the problems that arise when estimating BSPs in the trunk, Pearsall et al. used CT on two males and two females to focus on the estimation of trunk BSPs (Pearsall et al., 1992; 1996).

More recently, Durkin (1998; 2002) used dual photon absorptiometry (DPX) to predict the mass, moment of inertia, and centre of mass location of human limb segments. DPX measures the attenuation of two high energy photons as they pass through a body, and has become a standard clinical tool to measure bone density and body composition. The speed and accuracy of the DPX method has allowed Durkin to accumulate a large sample of data on living subjects. Using a large sample (100 subjects) to investigate the differences in BSPs between subpopulations, Durkin has shown differences in morphology between at least four populations (males and females, ages 19-30, and 65+). This observation has led to the development of population specific regression equations. Durkin has shown that population specific regression equations are more accurate than previous general equations for BSP estimation when compared to DPX measurements (considered to be accurate) (Durkin, 1998).

The most obvious problem with the use of some medical imaging technology in anthropometry studies is that the equipment can expose living subjects to radiation. While radiation exposure to the subject is less than that from CT, both DPX and gamma-

ray scanning only produce an image in two dimensions. This means the researcher must develop a technique to infer the third dimension, or use a tool that directly produces a three dimensional image, while minimizing radiation exposure. Magnetic resonance imaging (MRI), which maps the bonding state and relative concentration of hydrogen atoms, is a clinical tool that can produce a three dimensional image of a subject, while exposing that subject to a low level of radiation (Pearsall and Reid, 1994).

Martin et al. (1989) used MRI on eight baboon cadavers to measure segment mass, density, centre of mass, and moment of inertia. The MRI results were then compared with those observed using existing methods (i.e. those used in cadaver studies). In a later study, Martin compared MRI with other methods for estimating BSPs in 12 adult males (Mungiole and Martin, 1990). These studies led Martin to believe MRI capable for measuring BSPs accurately.

The drawback to MRI is that since it cannot directly measure tissue density, it assumes density values as calculated using other means (such as from cadaver studies). Upon meticulous investigation of MRI cross sectional images, Martin was able to distinguish between areas of bone, fat, and muscle tissues throughout the body (Martin et al., 1989). Like Jensen, Martin noticed the need for density profiles, and argued that the density profile of a segment is highly sensitive to the modeling of bone tissue (Mungiole and Martin, 1990). Thus, the assumption of uniform density within a segment will greatly affect the estimation of BSPs.

Both medical imaging technology and the studies using it for BSP estimation show limitations in addition to those stated. For instance, Zatsiorsky and Seluyanov's (1983) study was performed on young males. Durkin's observation of BSP differences between males and females, elderly and young, show Zatsiorsky and Seluyanov's (1983) results may not be representative of a larger population. As well, some of the studies were not performed on humans, which again, does not make them relevant to predicting human BSPs. While many of the cited researchers believe imaging technology to be an accurate method in predicting body segment parameters in the subjects scanned, it is quite impractical for a number of reasons. For one, it is quite expensive. Also, scanning subjects and processing data is often quite time consuming.

Mathematical and Geometric Models

For the reasons noted above, water immersion, photogrammetry, and the use of medical imaging to estimate BSPs is either inaccurate due to assumptions in density, or iIt is reasonable to state that methods previously mentioned for estimating the BSPs of an individual are, for reasons of cost, time, or technical expertise, beyond the means of many researchers and clinicians. This has led to the need for a quick, inexpensive and reliable method. One method is the creation of mathematical models (ie. regression equations) in order to predict body segment parameters.

One researcher to recognize the utility of mathematical models was Hinrichs (1985), who used data from Chandler et al. (1975) to develop linear regression equations to predict a subset of BSPs from anthropometric measurements. One limitation with Hinrichs' study is that he assumed symmetry for each segment about its longitudinal axis. As well, Hinrichs warns that due to the small sample size, one should be cautious about predicting BSPs of subjects that have anthropometric measurements falling outside the sample (in this case the cadavers used in Chandler's research) value range (Hinrichs, 1985).

The most popular and widely used of the mathematical models is that created by Winter (1990). Winter used data collected by Dempster (1955) to create tables that predict BSPs. Winter's tables allow the user to predict a particular segment's mass from whole body mass, the segment's length from whole body height, and centre of mass and radius of gyration from the length of the segment. The tables created by Winter are limited in that they are based on cadaver data, which, as stated above, is not representative of living subjects, nor does it take into account gender, age, and cultural differences. As well, these tables assumed perfect symmetry of the human body. A recent study by Durkin (1998) has revealed the Winter tables poorly estimate many BSPs. In contrast to Winter's tables, the population specific regression equations based on living subject data have produced superior results (Durkin, 1998).

Though population specific anthropometric tables are better for calculating human BSPs than the previous tables by Winter, this method requires the user to have four sets of tables, each specific to a sub-population. Recognizing this, researchers began to look for geometric similarity among populations. If similarity exists, a geometric solid, which could be created for a segment with the collection of a few simple measurements, may explain the inertial characteristics of the limb segment modeled regardless of age and/or gender.

Harless was the first to use a geometric model in order to estimate the inertial characteristics of a body segment (Pearsall and Reid, 1994). The trunk of one cadaver subject was represented as a cylindrical object. Unfortunately Harless' model does not apply to a larger population due to the small sample size.

The next attempt at a geometric model was by Hanavan (1964). Based on the anthropometric data collected by Dempster (1955), Hanavan developed a series of ellipses, spheres, frusta, and cylinders to represent the shape of specific body segments. While his predictions for centre of mass and moment of inertia were good, his study is limited to the cadaver sample.

Zatsiorsky et al. (1990) conceived a method to create geometric solids that were cylindrical in shape using data collected by a gamma-ray scanner. His method requires the user to take a few measurements, such as length and circumference of the limb in question, and then use equations to calculate segment mass and moment of inertia. These

calculations are based on the assumption that each limb can be modeled as a cylinder of specific length and diameter based on a measured length and circumference. Unfortunately, Zatsiorsky's results are limited to a sample of young, fit, and male.

A recently published geometric model by Durkin (1998) showed that differences exist between subpopulations. Thus, Durkin states that a good geometric model must account for these differences. Durkin then defined models of various shapes for each segment. By assuming a constant density, these models could estimate mass, centre of mass, and moment of inertia in three dimensions. The results were inconclusive. That is, BSPs could be predicted in some segments, while other segments had poor estimates of some of their BSPs. As well, population specific linear regression equations based on the same data tended to better estimate BSPs (Durkin, 1998).

It has been noted that geometric models fail since they assume uniform density for a segment. It has been noted by Jensen and Martin that density changes throughout a segment, and that there is a need for a segment density profile (Wei and Jensen, 1995; Mungiole and Martin, 1990). Proper choice of shape may account for density issues. That is, if a constant density is assumed, one can increase the mass for a region of a segment by increasing the volume in that region. For example, the arm increases in density at the distal end. In order to compensate for this, the volume of the shape used to represent the arm must be increased at the proximal end. This leads to more complicated shapes.

The complication of shape due to non-uniform segment density led Hopkins (2002) to examine the human body on a slice by slice basis. Using images from the Visible Human Project (Spitzer and Whitlock, 1998), Hopkins examined whether uniform density ellipses could be fit to represent the mass distribution of 20 transverse plane slices. If performed on a larger sample, it is thought that the stacking of such ellipses will allow for the creation of a geometric shape that more closely follows the contours of the segment. Hopkins found that some of the visible human slices (taken in the transverse plane) could be represented using ellipses, while others could not (Hopkins, 2002).

Future of Anthropometry

Studies to date have shown an evolution in the estimation of BSPs. This evolution has been the result of challenges of previous findings and the implementation of new technologies. While anthropometric models to this point have been deemed practical, they can inaccurately estimate a given person's BSPs. Few studies have shown the ability to predict BSPs in a large and varied population.

Understanding of the limitations of previous models, and knowledge that subpopulations exist should encourage the need for more representative models. Also, new technology has allowed for examination of the human body with greater precision.

Future studies should take advantage of modern techniques to address the limitations of previous studies.

Creating a three dimensional model

Biomechanists need information on segment mass, centre of that mass in the three principle axes (medial/lateral, anterior/posterior, and superior/inferior), and moment of inertia about those axes in order to understand the kinetics and kinematics of human movement (see appendix A for nomenclature used in this paper). The purpose of this study was to create a three-dimensional model to estimate these in the human body. Dual photon absorptiometry (DPX) can be used to measure body mass. Unfortunately, DPX can only provide information in two dimensions. Thus, one can only calculate centre of mass in both the medial/lateral and superior/inferior axes, and moment of inertia about the anterior/posterior axis. Magnetic resonance imaging (MRI), on the other hand, provides a three-dimensional representation of the body. While volume and tissue distribution can be measured, MRI is not able to directly measure mass. Therefore, DPX and MRI may be used together to provide information for calculating those BSPs that cannot be estimated from DPX alone. These BSPs are centre of mass in anterior/posterior axis, and moment of inertia about both the medial/lateral and inferior/superior axes.

In order to create a three-dimensional model using DPX and MRI, it is important to establish a relationship between a DPX scan of, and MRI images produced for an individual. This is the purpose of the first study. Assuming that a relationship is found between MRI and DPX, the purpose of a second study is to define a uniform density, elliptical representation of transverse plane slices so that a third dimension may be inferred from DPX slice measurements. Finally, a third study will compare uniform density ellipses created using MRI images with those derived using photogrammetry. If a relationship between MRI and photogrammetry can be found, it may be possible to bypass the expensive and time consuming step of producing and analyzing MRI images. Uniform density ellipses generated from photogrammetry could then replace those created using MRI images for the purpose of inferring a third dimension on DPX. Again, if mass and mass distribution could accurately be measured, one can calculate BSPs in three dimensions.

Study 1
A method for measuring mass using Magnetic Resonance Imaging

Purpose

Past studies have used medical imaging technology to estimate the inertial characteristics of human body segments. Bone density scanners, such as gamma-ray scanners and DPX, have been shown to accurately measure mass directly. Unfortunately, bone density scanners do not produce a three-dimensional image.

Magnetic resonance imaging technology (MRI) has the ability to produce a three-dimensional image. MRI is limited in that it does not directly measure tissue density or mass. Between the two technologies, DPX and MRI directly measure mass, volume, and provide an image of the body in three dimensions. Using this information, one may be able to examine mass distribution in three dimensions. The purpose of this study is to test a method to calculate three-dimensional mass data from an MRI scan on a human subject. DPX will be used to validate the results of the MRI method.

Equipment

Dual Photon X-ray Scanner (DPX)

DPX is widely used clinically to measure bone density while exposing the subject to a low level of radiation as compared to other imaging technologies (i.e. $1/10^{th}$ that of a chest x-ray) (Webber, 1995). The subject is placed on the bed, and a collimated beam emits photons of two different energies at the subject in a serpentine manner, head to toe. DPX technology measures density based on the probability of a photon emitted from the scanner being absorbed or scattered by body tissue. A detector measures the attenuated intensity after the photons have passed through the body (Durkin, 1998). Measured intensities are calibrated using a phantom (scanned along with the subject). The phantom approximates the attenuation coefficient for soft tissue, bone, and air at each photon energy level (Webber, 1995).

The scanner used in this study is the Hologic QDR-1000. This scanner emits photons of two significantly different energies (70 keV, and 140 keV). A collimated beam emits photons from below the subject. A moving scanner arm (located directly above the subject) in line with the beam detects the emitted photons. A calibration wheel, resting between the subject and the x-ray source, provides an automatic internal reference system (Hologic QDR-1000 Operators Manual, 1989; Durkin, 1998).

Calcium atoms (present in bone) are likely to interact with photons of both low and high energy. On the other hand, carbon atoms (present in soft tissue) are more likely to interact with only higher energy photons (Webber, 1995). The measured intensity values of higher energy photons are thought to be reflective of body mass. This is due to the fact that higher energy photons interact with all atoms with relative equality. Mass data was extracted from the raw DPX data using the attenuation of the 140 keV beam, and calibrated using software (Durkin and Dowling, 1998).

Magnetic Resonance Imaging (MRI)

MRI works by imaging an unstable portion of a subject's own magnetic field. The stable magnetic field in the subject is produced through the use of a strong, uniform magnet. MRI uses three types of magnets (resistive, permanent, superconducting) to produce a magnetic field around the subject. Once the subject's magnetic field is aligned with the magnetic field produced by the magnets, equilibrium is established. Next, specific frequency radio waves are applied to a specific region in the subject, and this disturbs the subject's magnetic field by rotating it away from equilibrium. Cessation of the radio waves allows the subject's field to realign with the field produced by the magnet. As this happens, radio waves released by the atoms in the targeted tissue are "echoed" back to a sensor on the scanner. Signal position information is encoded using switchable magnetic gradients. The amplitude of the echoed radio waves determines the brightness of the image produced for the region scanned (Friedman et al., 1989).

The head scan used a radio wave repetition time of 505 ms and an echo time of 15 ms to produce T1 weighted images. The slice thickness used was 5 mm with a gap width of 2.1 mm. White matter was used as a reference tissue. The rest of the body was scanned with a repetition time of 400 ms and an echo time of 15 ms to again produce T1 weighted images. Again the slice thickness was 5 mm with a 2.1 mm gap width. The reference tissue used was skeletal muscle for all scans (excluding head scans).

Subject

The subject of this study was a young, fit, 25 year old male. Digitization (for both the DPX and MRI methods) was not done on the whole body. Regions covered in this model were the head/neck, the trunk, and the right leg. The arms were included as part of the trunk until the point where the arm can be distinguished as being separate from the trunk. As well, both legs were considered part of the trunk until it can be judged with certainty that the leg was separate from the trunk, at which point, the digitization method continued down the right leg. Therefore when this paper discusses the whole body, the data excludes both arms and the left leg.

Digitization was also done on the right arm. The arm was considered the point at which the arm is clearly separate from the trunk to the wrist. Hand data was excluded due to the resolution of hand images in both the MRI and DPX scans. Arm data was not included in the whole body analysis due to the fact that the arm data runs concurrently with trunk and thigh data. Since, most graphs in this study display slice data in a head to ankle manner, the only place for arm data would be at the end of each plot. It was felt that this would confuse the reader, so arm data has been analyzed apart from what has been considered whole body in an attempt to keep the message clear.

Methods

The subject was first scanned using DPX. For the subject, DPX scanned 146 lines head to toe (along superior-inferior axis), with 112 samples per line (along medial-lateral axis). The data was then organized into transverse slices at the point of each scan line. Within each slice, the 112 samples were organized into columns 5.31 mm apart. The depth of each slice was assigned a value of 13.16 mm, the distance between each scan line along the superior-inferior axis. The DPX scanner measured the mass of each element.

The mass of each column was plotted against the column position along the transverse plane for each slice. This data yielded a three dimensional representation of the body mass to produce a 'MASSMAP' of the body. The mass of each slice was calculated by summing the column masses within the slice. The entire DPX method is diagramed in figure 1 (Appendix B).

The subject was also scanned using MRI. The body was scanned in a number of overlapping series. Using landmarks to eliminate redundant slices due to the overlapping, the MRI produced 271 transverse plane slices, head to toe. The next step was to decide which of the 271 MRI slices would match up with the slices produced by the DPX. A number of landmarks, such as the greater trochanter and the right knee joint centre, were used to match key MRI slices with their DPX equivalents. MRI slices in-between these landmarks were matched up with DPX slices on either a 2:1 or a 3:2 basis depending on location within the body. That is, in some locations every other MRI slice was chosen, whereas in other locations 2 MRI slices were chosen and then one was skipped. This is due to the MRI being done in multiple series, with some regions of the body producing a higher density of transverse scans (i.e. more images produced per unit length). The discrepancy is also due to MRI images not being taken at exactly 13.16 mm apart. The foot remained unmatched due to differing foot position in each scan, thus the final result was 133 MRI slices matched with 133 DPX slices. Slice widths were also measured to assist in this procedure.

MRI slices were digitized in order to calculate mass. Each slice was sectioned into columns 9 pixels (11.25 mm) across. Since each MRI slice is treated as equivalent to a DPX slice, each slice (and thus column) was assigned a depth of 13.16 mm. Further subdivision by height within each column was done according differing tissue types, as shown in figure 1.1.

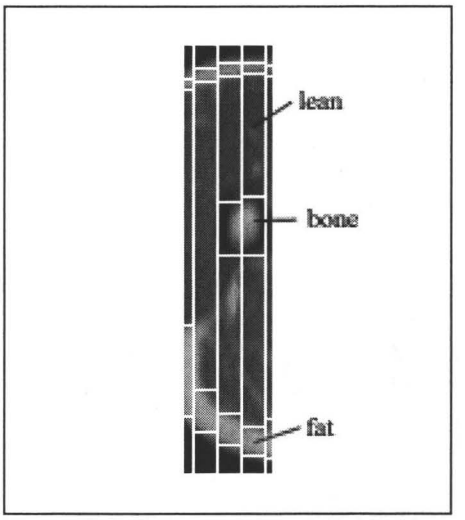

Figure 1.1: Columns are subdivided into different tissues

The mass of each subdivision within each column was calculated using the following equation:

$$H \times 1.25 \times 11.25 \times 13.16 \times D \times 10^{-6} \quad [1]$$

...where H is the height of each subdivision in pixels, 1.25 is the conversions factor from pixels to mm for the height measurement, and 10^{-6} is the converts the result into metres. D is the density of the tissue. This model separates the body into four different tissues types; lean, fat, bone and brain. Bone tissue was assigned a density value of 1.8 g/cm^3 (Clauser et al. 1969). Lean and fat tissues were assigned density values of 1.1 and 0.9 g/cm^3, respectively (Siri, 1956). The DPX assumes the brain to be lean tissue with 17% fat composition; therefore a density value of 1.066 g/cm^3 was assigned. Gas pockets in the intestine and spaces in the lungs were considered air, and were given a density of 0 g/cm^3 (making up the fifth component of the five component model).

The mass of each column was summed, and the column masses were plotted versus the column position across the medial/lateral axis for each slice. The mass of each slice was calculated by summing the column masses within each slice. The MRI method is diagramed in figure 2 (Appendix B).

MRI arm images were matched up with their equivalent DPX data using the same process as for the rest of the body. Mass information was derived using the MRI digitization process in the same manner as for the rest of the body. Arm information is presented separate from the rest of the body (as described above).

Statistical Analysis

With 133 transverse plane images being produced by both the DPX and MRI scanners, the sample size was considered to be 133 for the whole body. The statistical analysis consisted of percent root mean square (%RMS) error calculations when comparing MRI slice mass estimates against DPX measurements. RMS error calculates the average percent difference between the MRI slice estimates and DPX slice measurements. As well, a scatter plot comparing individual slice mass estimates for MRI versus DPX was produced. A Linear regression equation was developed and an R^2 value was calculated.

Thirty-two images made up the arm. Therefore the sample size for the arm is 32. The arm was subject to the same statistical analysis as the whole body.

Results

Whole Body

When comparing MRI slice mass with DPX slice mass, an RMS error of 12.5% was calculated. In total, the MRI digitization overestimated whole body mass by 9.43%. Figure 1.2 compares slice mass for both DPX and MRI methods from head to ankle. An R^2 value of 0.9707 was calculated for the DPX mass versus MRI mass. Figure 1.3 displays the scatter plot comparing the MRI mass estimate for each slice against its DPX measurement.

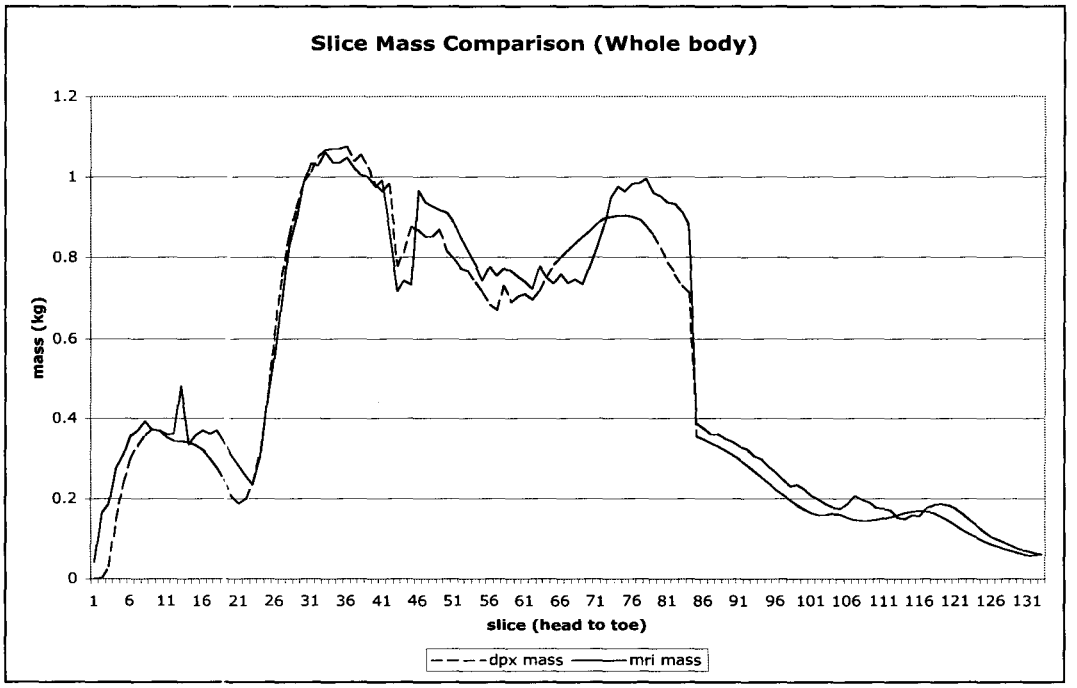

Figure 1.2: plotted slice mass for MRI and DPX. Slice mass compared starting from top of head and moving down through the body to the ankle. The area under each curve represents the whole body mass.

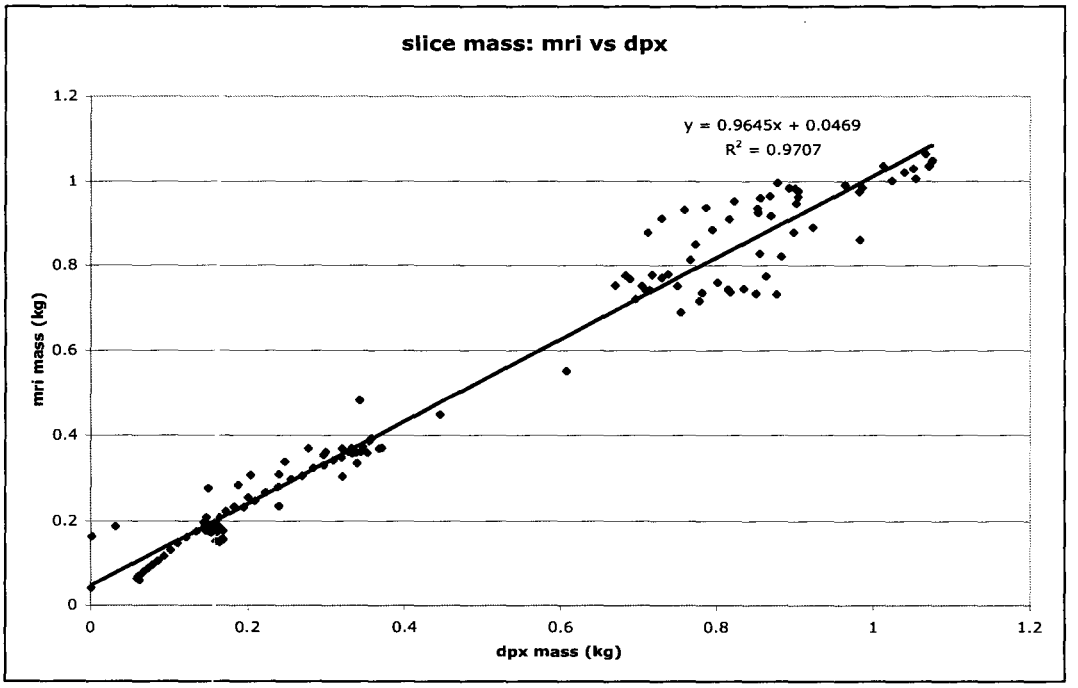

Figure 1.3: MRI slice mass estimate vs. DPX slice mass measurement scatter plot.

The plots of column mass versus column position in the medial/lateral axis created mass profiles for both DPX and MRI slices. A qualitative analysis was performed on these profiles. Appendix C shows examples of both DPX and MRI slice profiles taken throughout the body. The columns are plotted across the medial/lateral axis right [side of the body] to left. The area under each curve represents the total mass of the slice plotted.

Arm

MRI slice mass estimates show an RMS error of 23.5% when compared to DPX slice mass measurements for the arm. Figure 1.4 compares MRI and DPX slice mass estimates for the arm, proximal to distal. A scatter plot comparing MRI slice mass estimates against their DPX measurements is displayed in figure 1.5. An R^2 value of 0.4975 was calculated for the arm slice mass comparison.

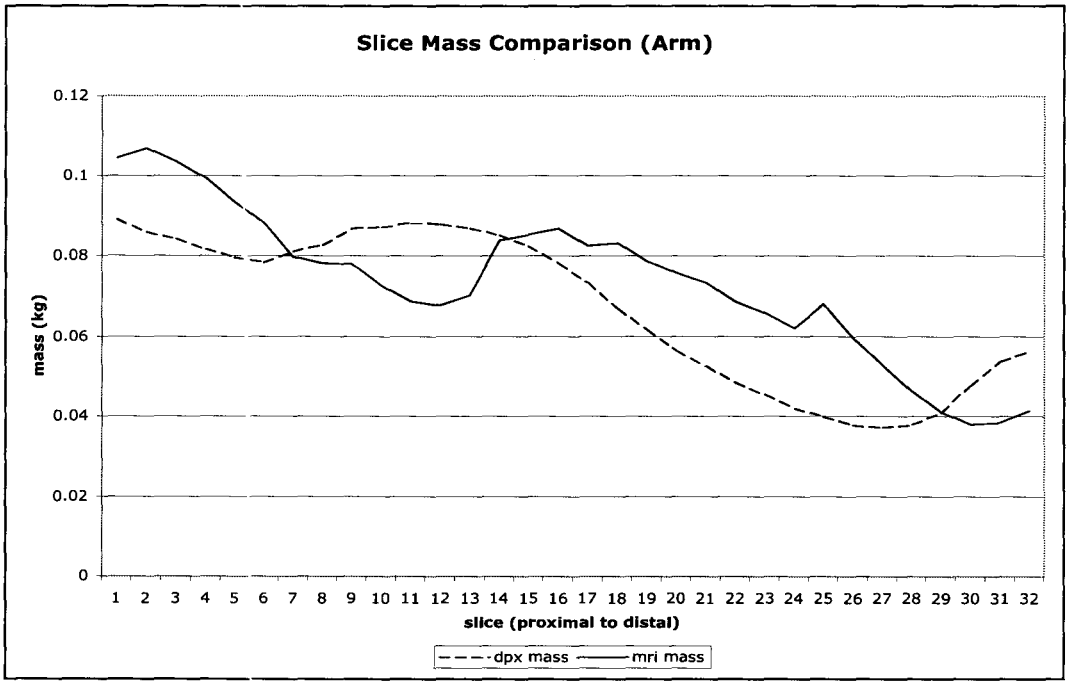

Figure 1.4: Slice mass for DPX and MRI. Slice 1 is the point at which the arm appears separate from the trunk. Slice 32 is the wrist joint centre (right arm).

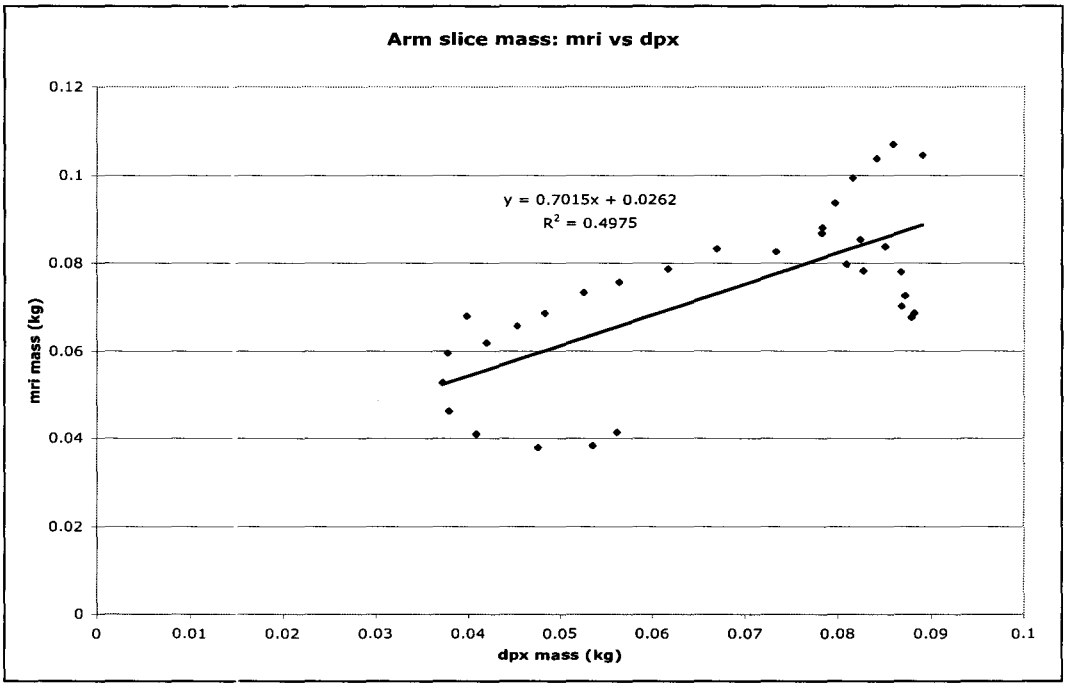

Figure 1.5: Arm MRI slice mass estimate vs. DPX slice mass measurement scatter plot.

Discussion

DPX has been shown to be an accurate method for measuring mass, and distribution of mass in a human subject (Durkin, 2002). With this in mind, the DPX results for slice masses, and slice mass profiles in the medial/lateral axis are accepted as being accurate. The R^2 calculation of 0.9707 shows a strong correlation between MRI estimates and DPX measurements for slice mass. While the DPX and MRI mass curves in figure 1.2 follow the same pattern, one can see that MRI seems to consistently overestimate mass throughout the body. This overestimation is, at worst, 0.2 kg for an individual slice (lower abdomen). The reason for the overestimation may be due to an inaccuracy in the MRI digitization procedure. Overall, MRI scans have a poor resolution; that is, many tissues were not easily distinguishable. It may be that a higher resolution scan, or an adjustment of tissue densities may bring the mass discrepancy to a minimum. Also, digitization using greater than a 5-component model (lean, fat, bone, brain, air) may improve results.

This study is concerned with two things: 1) the distribution of the mass throughout the body on a slice-to-slice basis, and 2) the distribution of the mass within a slice, across the medial/lateral axis. Having seen that MRI overestimates mass for individual slices, the mass profiles in Appendix C provide insight into why this discrepancy exists. For most of the profiles, the DPX and MRI curves follow the same shape, with only slight deviations. For example, slices 28 and 36 bothl have 3 peaks, with depressions between the peaks representing the lungs. The central peak in all three slices seems to be higher in the MRI profiles than in the DPX profiles. This may be due

to an inaccurate estimation of spine mass. The spine was digitized as being bone, yet the intervertebral discs, which comprise much of the spine, do not have the same density as bone. Also, each vertebra has an opening for the spinal column, again, lowering the density of the spine. Due to the poor resolution of the MRI images, accurate digitization of both the intervertebral disc and the spinal column was not always possible, and was ignored for the sake of consistency in the method. Due to these facts, it is reasonable that an adjustment to the density assigned to the spine will bring the mass distribution, and thus the total mass of the slice, more inline with the true distribution (i.e. the DPX profile). This phenomenon can also be seen in slice 61, where the MRI profile has a bump in the middle of the curve while the DPX profile does not.

On occasion, qualitatively, some of the slices showed large variability in the mass distribution between the DPX and MRI profiles. This occurs in the transition zones between body segments. Slice 26, which is located between the head/neck and the trunk segments, was included in Appendix C to illustrate this occurrence. The variation between the DPX and MRI profiles may be due to inconsistencies in body position between scans, which transition zones (regions between segments, such as joints or the neck) are much more prone to. Also, variability may again be due to the inability to accurately distinguish between tissues in the MRI because of the poor resolution of the images.

The low R^2 calculation of 0.4975 for the arm shows a large discrepancy between the MRI digitization method estimates and the DPX measurements for slice mass. The slice mass difference may be due to the same reasons as explained for the transition zone discrepancies. As noted, transitions zones are susceptible to changes in body position between scans. An examination of figure 1.4 shows a possibility of MRI slices being matched with DPX slices 4 or 5 slices distal to their true matches. This may be explained by a change in arm position between scans (such as a shoulder shrug, or an arm abduction). A shift in the data to alleviate this problem was not possible due to the nature of the raw data. What is important is that such results illustrate the importance of sameness in body position between scans. Future studies should take note of this.

Conclusion

While MRI seems to overestimate mass, the distribution of mass between and within slices seems to reasonably follow the same patterns as those depicted by DPX. In order for the MRI digitization method to more accurately depict mass, the MRI mass profiles both between and within slices must follow the DPX distributions more exactly. This may be done by switching to a model that uses more than five components or by fine-tuning the tissue densities applied. If this can be done, one will be able to use MRI to calculate those BSPs that elude the two dimensional DPX image. The cost of an MRI scan is much higher and the digitization method is much more time consuming than the DPX method. Therefore it would be beneficial if future studies examined techniques that allow a three-dimensional model to be inferred from a DPX scan.

Study 2
Measuring BSPs using uniform density ellipses generated from MRI

Purpose

The time consuming and expensive nature of the proposed MRI digitization process prompted the need for a method in which one can obtain three dimensional information about human body segments without having to subject a population to MRI scans. The previous study (study 1) has shown that MRI may be used to estimate mass, and thus distribution of mass for transverse plane slices. Using this information, it may be possible to develop a three dimensional shape for each slice that estimates mass and distributes that mass in the same manner as the MRI images display.

Past studies, such as those using photogrammetry, have represented the body segments as being elliptical. As well, a glance at individual transverse plane images produced by the MRI scan show that slices appear to be elliptical in shape. The purpose of this study is to develop uniform density ellipses for each slice and compare BSPs (specifically mass, centre of mass in the medial/lateral and anterior/posterior axes, and moment of inertia about the superior/inferior axis) of such ellipses with MRI digitization estimates. If uniform density ellipses can be made to accurately depict the MRI estimates, the ellipses may be substituted for the MRI digitization process.

Subject

A 25 year old, fit male was scanned using Magnetic Resonance Imaging (MRI). The scan yielded 133 images in the transverse plane (as per study 1: methods). The body was separated in to whole body (excluding arms and left leg) and right arm. For information on the terminology regarding this study's definition of whole body and right arm see study 1 under the heading subject.

Methods

Each MRI slice was digitized to calculate mass using the method described in the previous study. This digitization method separates each slice into multiple rectangular prisms, each having its density (and therefore mass) defined by tissue type. An arbitrary axis was set on each scan, and the distance from the origin of this axis to the centre of the prism defined the centre of mass for each rectangular prism. Figure 2.1 describes how the axes were defined for each slice. The total mass of the slice was calculated by summing the masses of the prisms that make up each slice.

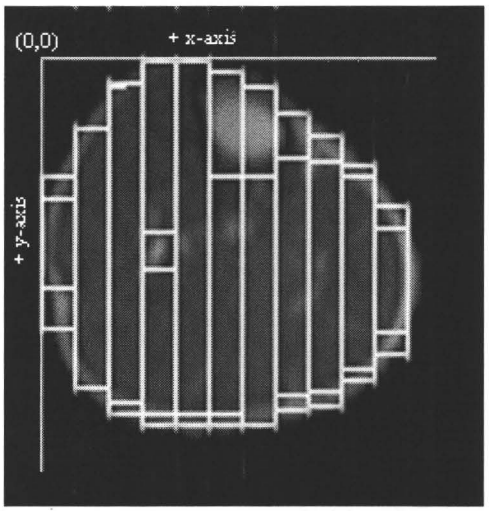

Figure 2.1: Defined axes on digitized MRI slice

The centre of mass in the x-axis (medial/lateral) for the slice was calculated using the following equation:

$$CofGx = \Sigma m_i x_i / M \quad [1]$$

...where m_i is the mass of a rectangular prism, x_i is the distance from the origin in the x-axis and M is the total mass of the slice.

The centre of mass in the y-axis (anterior/posterior) for the slice was calculated using the following equation:

$$CofGy = \Sigma m_i y_i / M \quad [2]$$

...where m_i is the mass of a rectangular prism, y_i is the distance from the origin in the y-axis and M is the total mass of the slice.

The moment of inertia for each rectangular prism was calculated using the following equation:

$$I_{CofGi} = 1/12m(h^2 + w^2) \quad [3]$$

...where m is the mass of the rectangular prism, h is the height and w is the width of the prism in millimeters. The moment of inertia about the centre of mass (about the superior/inferior axis) for the whole slice was calculated using the parallel axis theorem:

$$I_{CofG} = \Sigma(I_{CofGi} + m_i r_i^2) \quad [4]$$

...where r_i is the distance of the centre of mass for the rectangular prism to the centre of mass for the whole slice. This distance can be calculated using the following equation:

$$r_i^2 = (CofGx - x_i)^2 + (CofGy - y_i)^2 \quad [5]$$

Ellipses were created for each slice, and the mass of each ellipse calculated using the following equation:

$$Mass = \pi \times width/2 \times height/2 \times depth \times density \quad [6]$$

The width of the ellipse is the longest measured distance across the medial/lateral axis of the MRI slice. Height was defined as the longest measured distance across the anterior/posterior axis of the MRI slice. The depth of the ellipse is defined as 13.16 mm, which is the distance between MRI slices head-to-toe. Density was defined in three different ways. In the first case, a density of $1.1 g/cm^3$ was chosen (Siri, 1956). Lean tissue has a density of $1.1 g/cm^3$ and this value was chosen because a large portion of the body was defined as lean tissue in the MRI digitization process. The second case used a density profile as described by Winter (Winter, 1990). Figure 2.2 describes the density used for each section of the body. The third method used was a hybrid of the other two methods. All slices used a density value of $1.1 g/cm^3$ except for slices 32-45. These slice contained the lungs, and a density value of $0.92 g/cm^3$ was chosen based on the Winter anthropometric tables.

Regions	Slices	Density (g/cm^3)
Head and Neck	1-23	1.11
Chest (with shoulders)	24-30	1.00
Chest	31-45	0.92
Abdomen	46-77	1.01
Thigh	78-110	1.05
Shank	111-133	1.09

Figure 2.2: Density profile used in second (Winter) method for calculating ellipse mass.

Centre of mass in the x-axis was calculated as half the width of the ellipse, while the centre of mass in the y-axis was calculated as half the height of the ellipse. The moment of inertia about the centre of mass for each ellipse was calculated using the following equation:

$$I = 1/4m \times [(height/2)^2 + (width/2)^2] \quad [7]$$

...where m is the mass of the ellipse. The moment of inertia about the centre of mass was calculated using the mass from the lean tissue density, the Winter density profile, and the hybrid method.

The subject was also scanned using a Dual Photon X-ray scanner (DPX) as described in the previous study. DPX slice masses from the previous study were compared with the ellipses.

The entire process was repeated for the right arm. Since all three density profiles use the same value for the arm, a density of 1.11 g/cm^3 was chosen. Therefore, arm data is presented alone, to be included as the same whether one is using the lean tissue, Winter, or hybrid density profiles.

Statistical Analysis

Slice mass estimates for each method were compared to those measured using DPX. Uniform density ellipses generated using MRI (lean tissue, Winter, and hybrid profiles) were compared to estimates by MRI digitization for slice mass, moment of inertia, and centre of mass (x and y-axes). Percent root mean square (%RMS) values were calculated for each method comparison. As well, scatter plots were created comparing slice mass, moment of inertia, and centre of mass calculated using each profile with their DPX (for mass) and MRI digitized counterparts. A regression equation was developed for these scatter plots and an R^2 value was calculated.

In order to validate the reproducibility of the MRI digitization method, six slices were re-digitized by both the original researcher (intra-rater) and a research assistant (inter-rater). Calculations were performed for mass, moment of inertia, and centre of mass. An analysis of variance was done to compare repeat digitization data (intra-rater) with the original estimates. A separate analysis of variance was done for the inter-rater re-digitization.

Mass, moment of inertia, and centre of mass estimates from the re-digitization of each slice were plotted against the original estimates. A regression analysis was done, and R^2 values were calculated.

Results

Mass, centre of mass in the x and y axes, and moment of inertia about the centre of mass were calculated for each slice. Values for all three ellipse methods were compared to those calculated using the MRI digitization method for each slice. A summary of the calculated %RMS errors and correlation coefficients (R^2) are displayed in appendix D for each comparison.

Whole Body

Mass

When using the lean tissue profile, the ellipses showed an 18.7% RMS error when compared to the mass calculated using MRI digitization. The ellipses showed an 18.4% error when compared to the mass calculated by DPX. Figure 2.3 shows how the mass is distributed slice-by-slice, head-to-ankle, for all three methods. The regression analysis for the lean tissue profile showed calculated R^2 values of 0.9293 and 0.9448 against the MRI digitization and DPX, respectively.

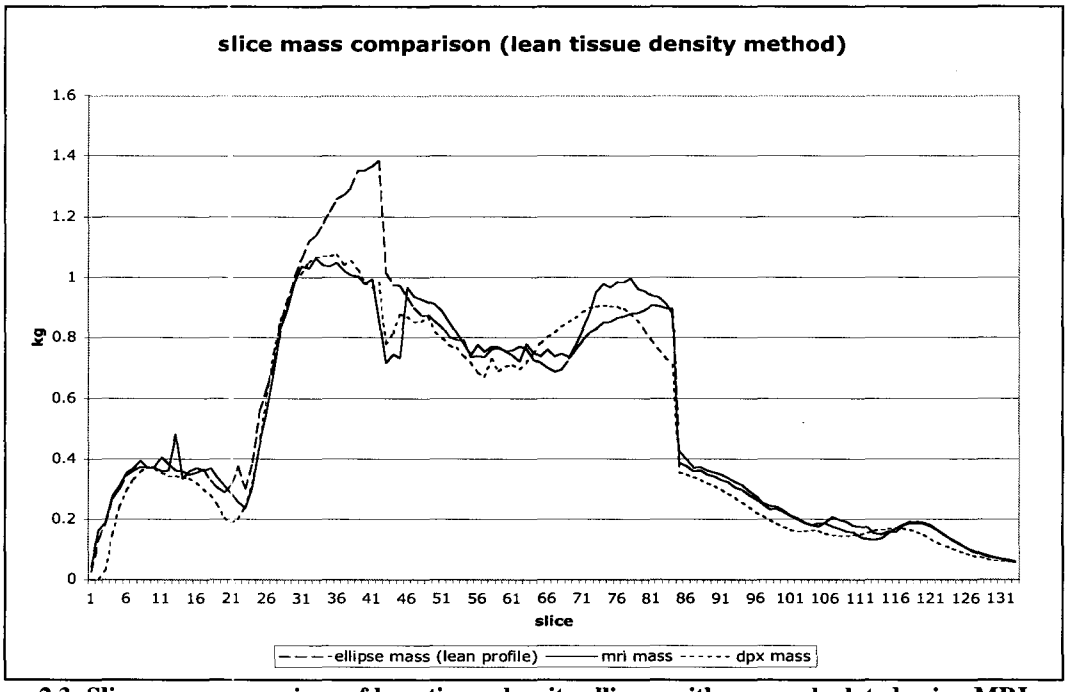

Figure 2.3: Slice mass comparison of lean tissue density ellipses with mass calculated using MRI digitization method and DPX.

When comparing ellipse mass calculated using the Winter density profile to mass calculated using the MRI method, the ellipses showed a 16% RMS error. When comparing these ellipse mass to that calculated using DPX, a 15.5% RMS error was seen. Figure 2.4 shows how mass calculated for ellipses using the Winter density profile compared to the mass calculated using the MRI digitization method and DPX for each slice. R^2 values of 0.9553 and 0.9546 were calculated when the Winter density ellipse slice mass estimates were plotted against their estimates using the MRI digitization method and their DPX measurements, respectively.

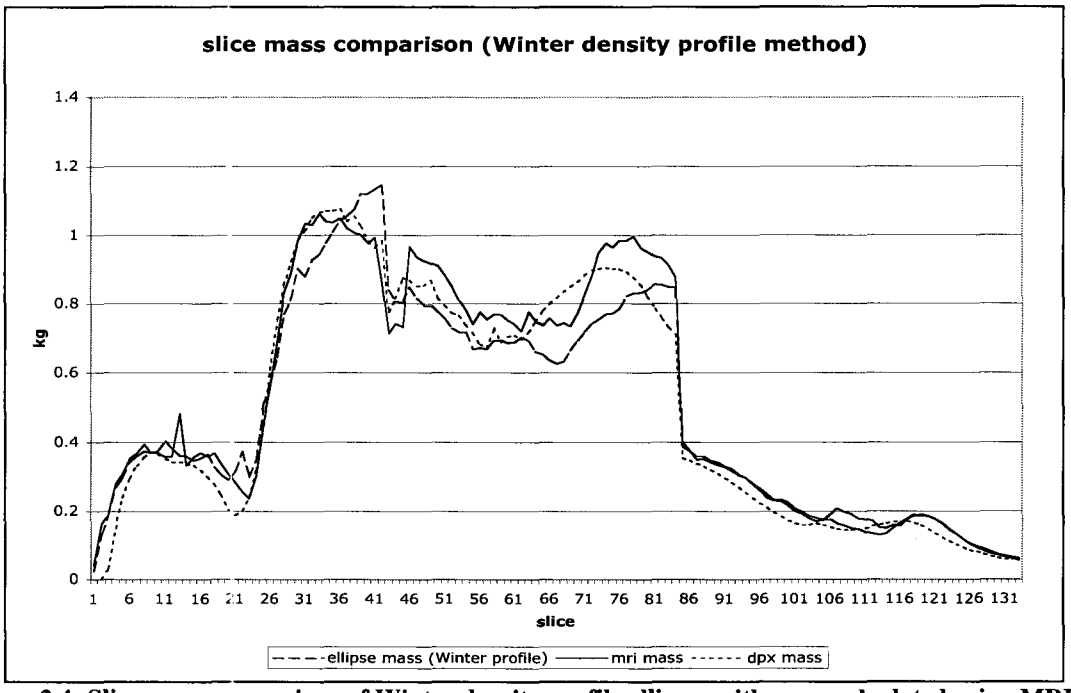

Figure 2.4: Slice mass comparison of Winter density profile ellipses with mass calculated using MRI digitization method and DPX.

Ellipse mass using the hybrid method was again compared to slice mass calculated using both the MRI digitization method, and that measured by DPX. The ellipses showed a 10.8% RMS error when compared to MRI masses, and a 13.1% RMS error when compared to DPX measured masses. Figure 2.5 shows the how the slice masses calculated using the hybrid method compare to those using the MRI and DPX methods. When the hybrid density profile ellipse mass estimates were plotted against their MRI digitized counterparts, an R^2 value of 0.9721 was calculated. An R^2 value of 0.9664 was calculated when the hybrid ellipse values were compared to DPX measurements for slice mass.

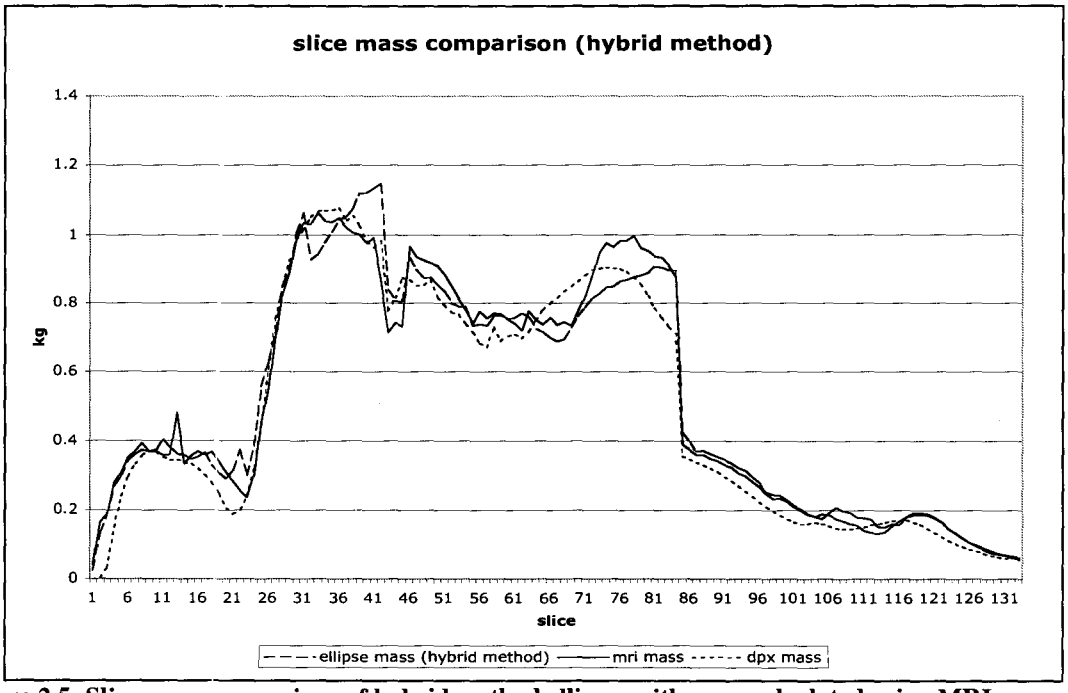

Figure 2.5: Slice mass comparison of hybrid method ellipses with mass calculated using MRI digitization method and DPX.

Centre of Mass

The centre of mass in the x-axis calculated using an ellipse had a 2.49% RMS error when compared to the centre of mass calculated using MRI digitization. The centre of mass for ellipses in the y-axis had a 6.96% RMS error when compared to MRI digitization calculations. Figures 2.6 and 2.7 show how ellipse centre of mass compares with MRI digitization calculation, slice by slice, in the x and y axes, respectively. In the regression analysis, R^2 values of 0.9981 and 0.9724 were calculated when the uniform density ellipse slice estimates were compared to their counterparts calculated using the MRI digitization method for centre of mass in the x and y-axes, respectively.

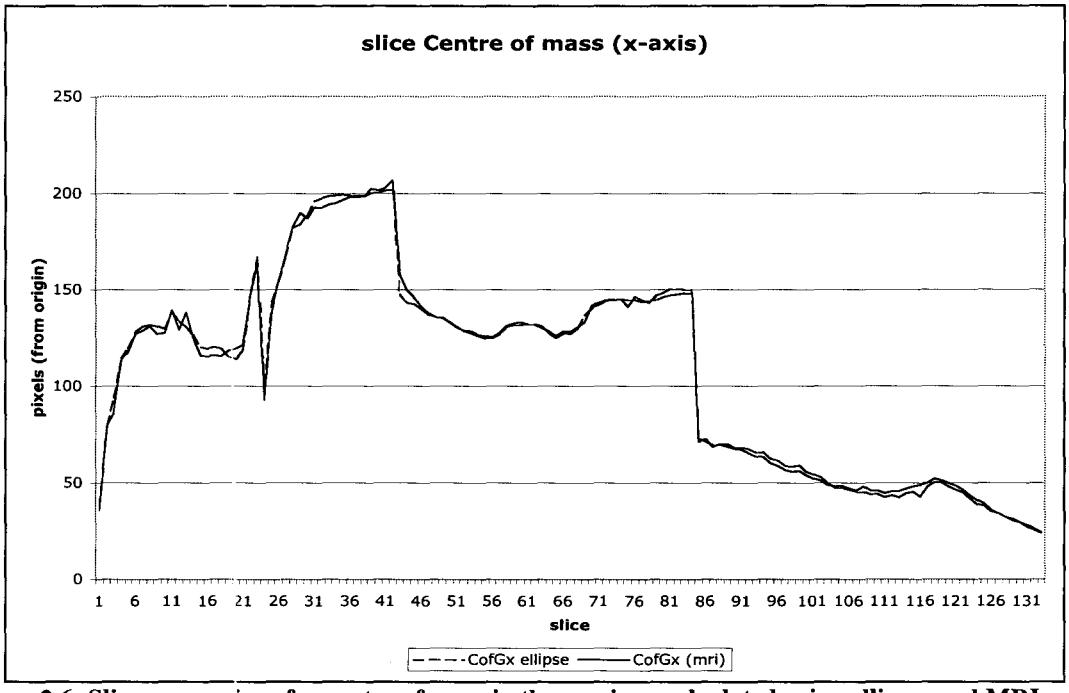

Figure 2.6: Slice comparison for centre of mass in the x-axis as calculated using ellipses and MRI digitization.

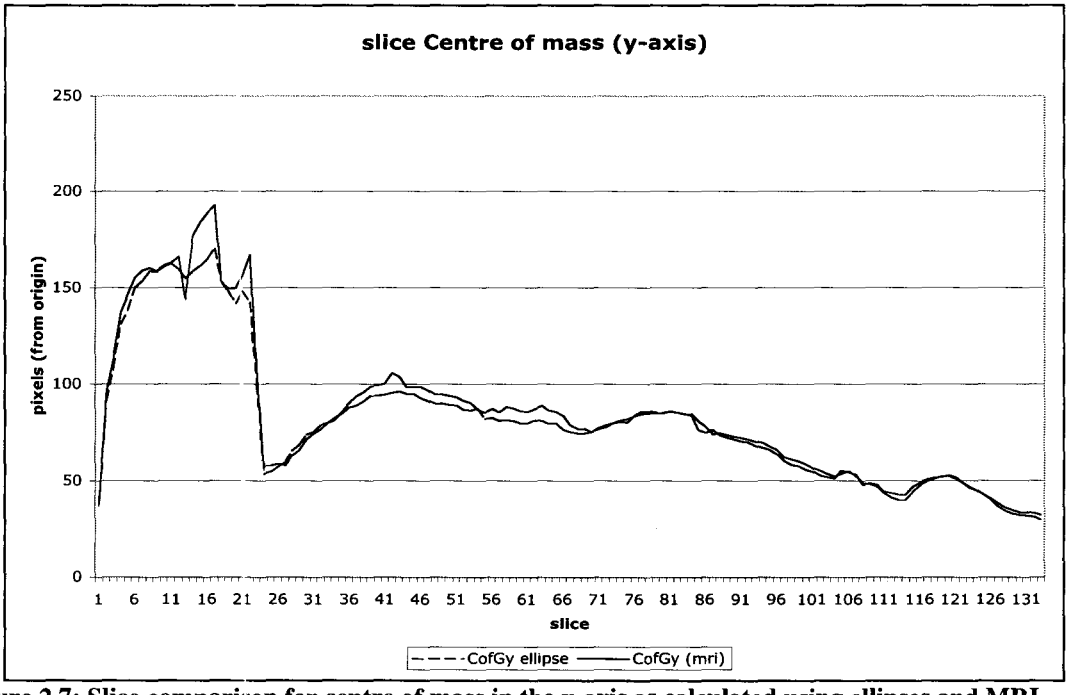

Figure 2.7: Slice comparison for centre of mass in the x-axis as calculated using ellipses and MRI digitization.

Moment of Inertia

Moment of inertia about the centre of mass for lean tissue density ellipses showed a 26.8% RMS error when compared to MRI digitization method values. The Winter density profile ellipses showed a 36.3% RMS error when compared to MRI. Figure 2.8 shows the moment of inertia profile, head-to-ankle, for all three methods. Both the lean tissue and Winter density ellipse slice moment of inertia estimates were plotted against the MRI digitization method calculations. R^2 values of 0.9529 and 0.9634 were seen for the lean tissue and Winter profiles, respectively.

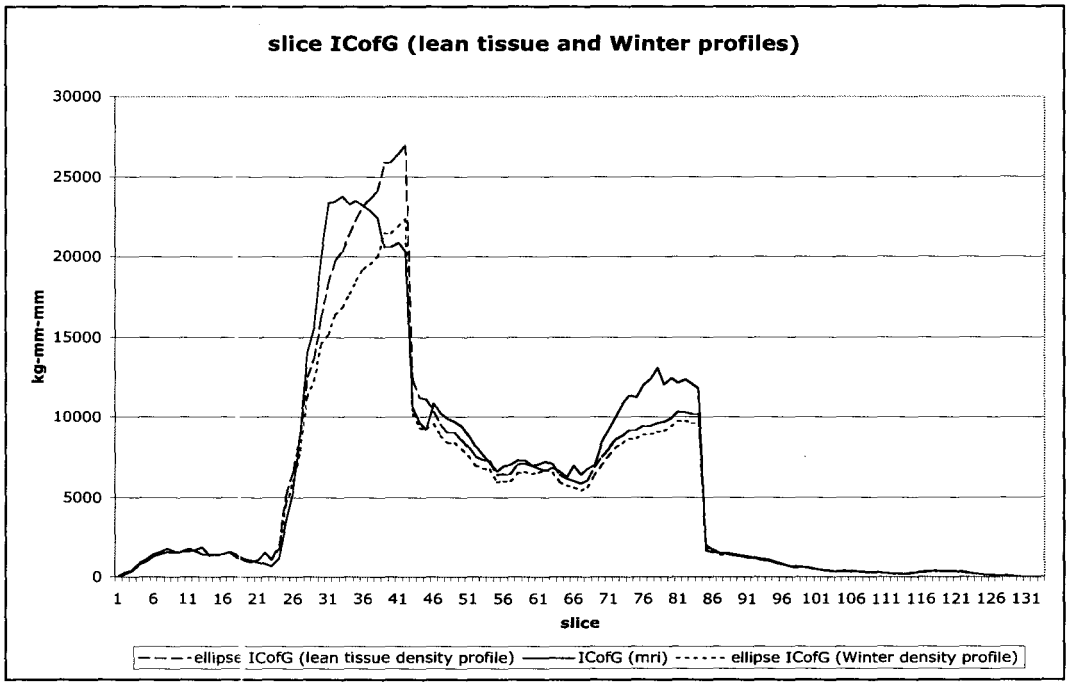

Figure 2.8: Slice comparison for moment of inertia calculations using MRI digitization method, lean tissue density ellipses, and ellipses created using the Winter density profile.

When using the hybrid method ellipse, slice moment of inertia about the centre of mass showed a 29.6% RMS error when compared to that calculated using the MRI digitization method. Figure 2.9 compares the hybrid method ellipse measurements with moment of inertia calculations using MRI. In the regression analysis, the hybrid model showed an R^2 value of 0.9701 when compared to MRI digitization method slice estimates.

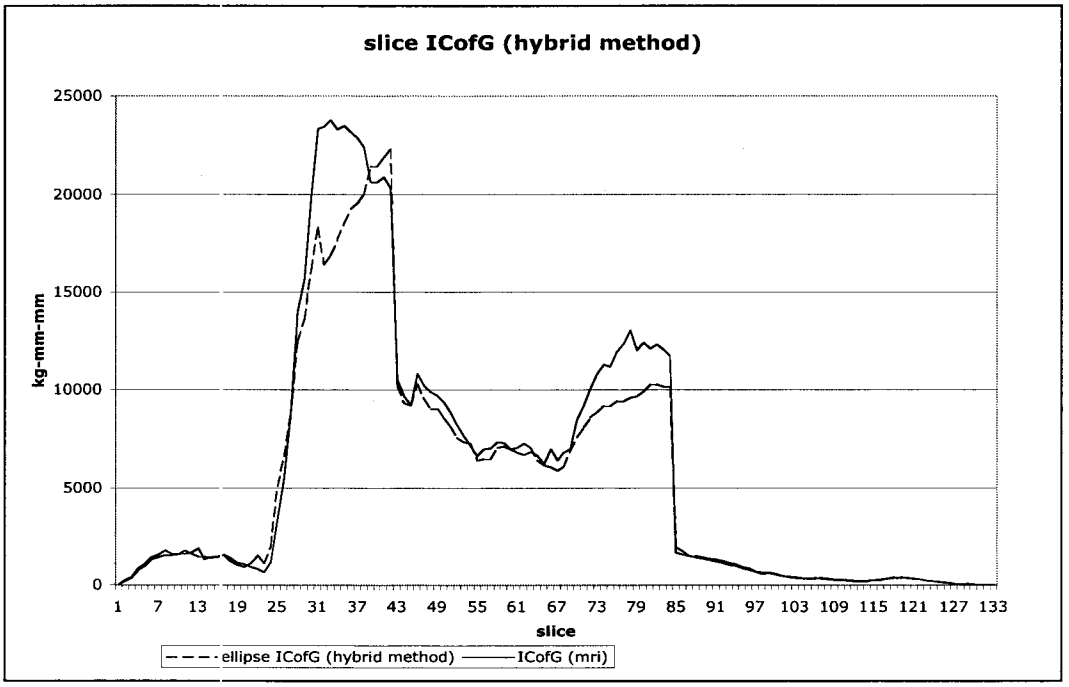

Figure 2.9: Slice moment of inertia about the centre of mass comparison. Ellipses were created using the hybrid method, and moment of inertia calculations were compared with those measured using the MRI digitization method.

Arm

Mass

When compared to DPX slice mass measurements, the uniform density ellipses show an RMS error of 28.1%. Compared to the slice mass calculated using the MRI digitization method, MRI ellipses showed an 8.34% RMS error. Figure 2.10 compares arm slice mass estimates for all three methods. R^2 values of 0.9485 and 0.4212 were calculated when the uniform density ellipse slice mass estimates were plotted against their estimates using the MRI digitization method and their DPX measurements, respectively

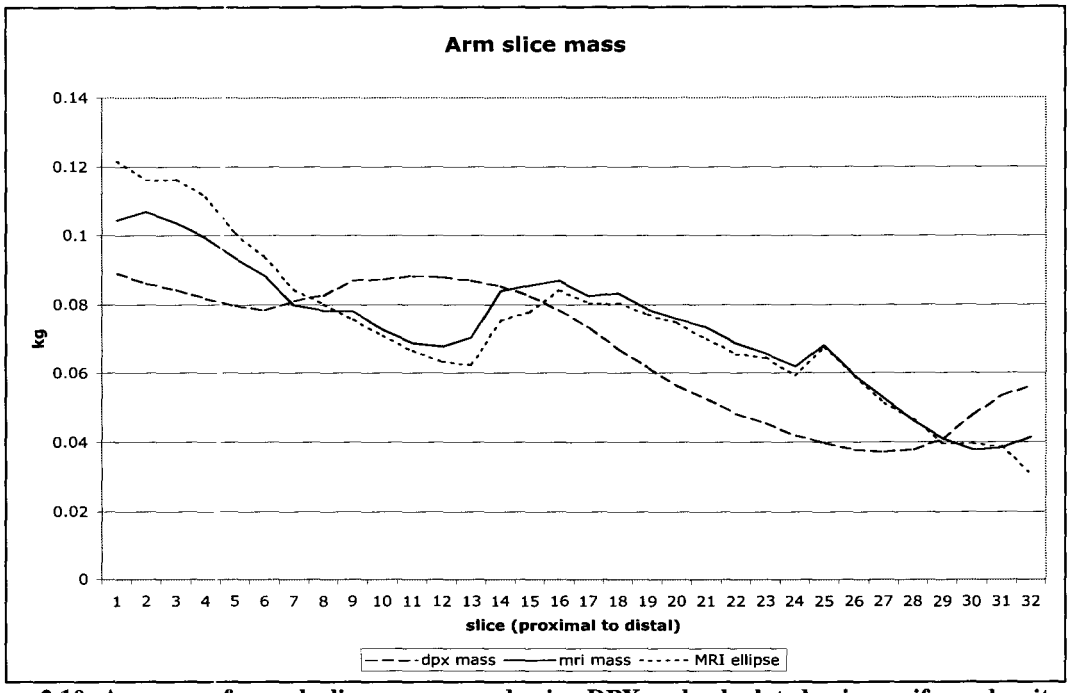

Figure 2.10: Arm mass for each slice as measured using DPX and calculated using uniform density ellipses and the MRI digitization method.

Centre of Mass

Centre of mass in the x and y-axes were taken as the distance from the origin for each slice. The slice centre of mass in the x-axis showed an RMS error of 6.91% when the ellipse calculations were compared to MRI digitization method estimates. Ellipse estimates for slice centre of mass in the y-axis showed a 4.19% RMS error when compared to those using the MRI digitization method. Figure 2.11 and 2.12 show slice centre of mass calculations for both the MRI digitization and ellipse methods in the x and y-axes, respectively. The uniform density ellipse slice centre of mass estimates were compared to those calculated using the MRI digitization method. R^2 values of 0.7549 and 0.9716 were calculated for the x and y-axes, respectively.

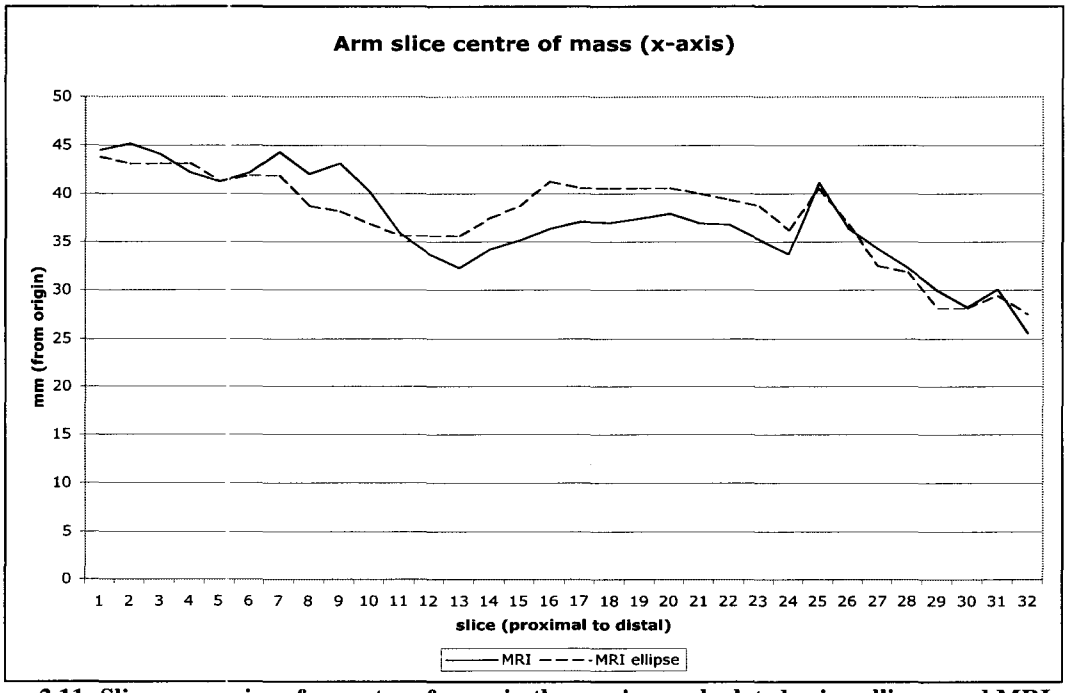

Figure 2.11: Slice comparison for centre of mass in the x-axis as calculated using ellipses and MRI digitization.

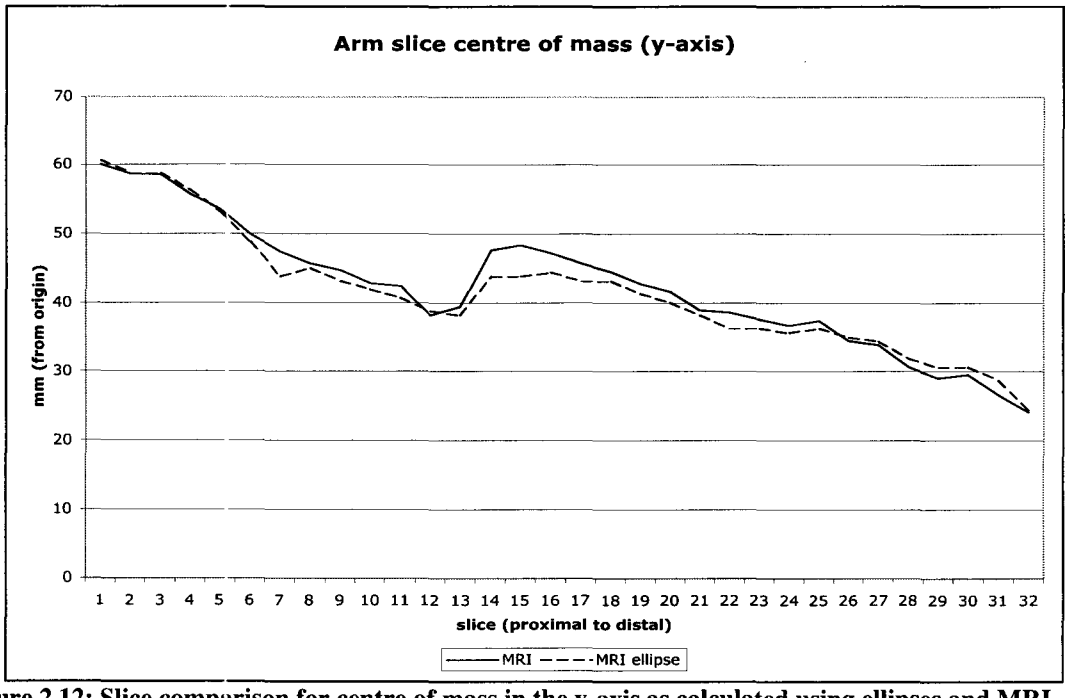

Figure 2.12: Slice comparison for centre of mass in the y-axis as calculated using ellipses and MRI digitization.

Moment of Inertia

The ellipses showed a 12.96% RMS error when compared to slice estimates using the MRI digitization method for moment of inertia about the centre of mass. The moment of inertia calculations for each method are compared in figure 2.13. The regression analysis produced an R^2 value of 0.9787 when the uniform density ellipse slice moment of inertia estimates were compared to those calculated using the MRI digitization method.

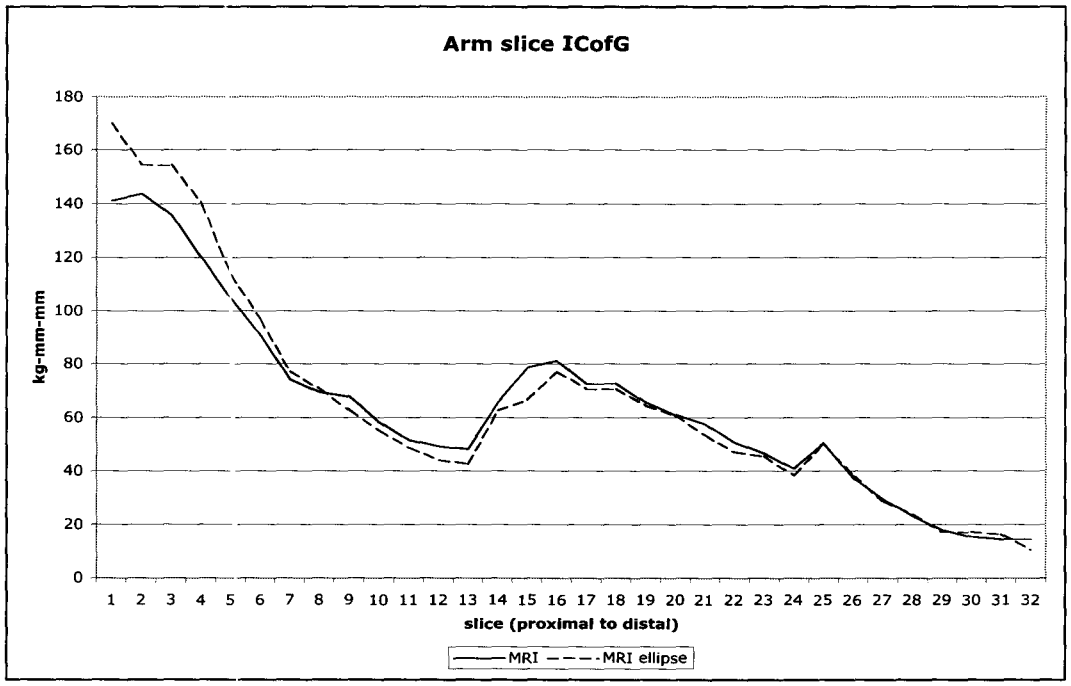

Figure 2.13: Moment of inertia (about centre of mass) estimates for each arm slice using ellipses and the MRI digitization method.

Validation of the MRI digitization method

Six MRI slices were re-digitized using the MRI digitization method in order to validate the method. Figure 2.14 and 2.15 show the raw data from the intra and interpersonal re-digitization, respectively.

Intra	Mass (kg)		ICofG (kg-mm^2)		CofGx (pixels)		CofGy (pixels)	
Slice	1	2	1	2	1	2	1	2
35	1.036	0.9969	23493.87	22241.15	196.83	189.59	86.216	86.357
46	0.9657	0.8130	10842.1	9074.77	141.09	137.70	98.612	97.642
71	0.8221	0.8146	9169.01	9339.03	142.94	143.20	76.750	76.669
77	0.9839	1.006	12362.82	12432.33	144.51	143.07	86.078	85.613
90	0.3409	0.3362	1280.495	1267.576	68.117	68.448	71.563	72.104
123	0.1463	0.1484	230.223	238.191	42.130	40.911	46.802	48.654

Figure 2.14: Intra-rater re-digitization data comparison. Column 1 is the original estimate, 2 the new (re-digitized) estimate.

Inter	Mass (kg)		ICofG (kg-mm^2)		CofGx (pixels)		CofGy (pixels)	
Slice	1	2	1	2	1	2	1	2
35	1.036	0.9354	23493.87	22423.13	196.83	195.24	86.216	86.624
46	0.9657	0.7833	10842.1	8886.19	141.09	139.14	98.612	96.806
71	0.8221	0.7950	9169.01	9232.42	142.94	143.37	76.750	76.666
77	0.9839	0.9922	12362.82	12435.31	144.51	144.45	86.078	85.191
90	0.3409	0.3377	1280.495	1263.807	68.117	68.447	71.563	71.378
123	0.1463	0.1451	230.223	231.087	42.130	40.890	46.802	48.533

Figure 2.15: Inter-rater re-digitization data comparison. Column 1 is the original estimate, 2 the new (re-digitized) estimate.

The analysis of variance ($\alpha = 0.05$) revealed no main effect for either the intra and inter-rater repeat digitization. That is, the variance created by the repeat digitization is not significant. The correlation assessment between slice estimates for mass, moment of inertia, and centre of mass and the estimates produced from the repeat digitization revealed R^2 values of greater than 0.96. Calculated R^2 values for the repeat digitization are presented in figure 2.16.

	Intrapersonal R^2	Interpersonal R^2
Mass	0.9733	0.9654
ICofG	0.9927	0.9916
CofGx	0.9985	0.9997
CofGy	0.9998	0.9989

Figure 2.16: Repeat digitization correlation coefficients.

Discussion

The high correlation coefficients (R^2 values all greater than 0.93) calculated for all comparisons done in this study show that uniform density ellipses may be used to represent transverse plane slices in the human body. The only exceptions to this are the comparison between the elliptical model's prediction of arm slice mass with DPX measurements and the arm x-axis centre of mass prediction for the uniform density

ellipses when compared to estimates from MRI digitization. The poor arm estimates with DPX may be due to difference in arm position between scans. As discussed in study 1, it seems that the MRI arm slices are 4 or 5 slices distal from their true DPX matches. As for the poor correlation between ellipses and MRI digitization for arm slice centre of mass in the x-axis, the error only accounts for a maximum 4 mm difference in position. For the most part, MRI image generated ellipses predict well when compared to the MRI digitization method's estimates (mass, centre of mass, moment of inertia) and DPX measurements (for mass).

Mass

The hybrid method showed the lowest %RMS values for slice mass estimates when compared to those calculated using the MRI digitization method and DPX. The RMS error for the hybrid model when compared to the other methods is around 10%; this translates to at worst a 0.15 kg error in slice mass estimation. Contrast this with the lean tissue and Winter profiles that can produce errors as high as 0.3 to 0.4 kg for slice mass. It is evident through the low %RMS error and the high R^2 value (compared to the lean tissue and Winter profiles), coupled with a qualitative analysis of figures 2.3-2.5, that the hybrid method is a better predictor of slice mass than ellipses using a lean tissue density or Winter density profile.

Centre of mass

When the two methods were compared, the slice estimates of the centre of mass in the x and y axes showed low %RMS errors. As well, the ellipses showed a nearly identical profile when compared to the centre of mass calculations using the MRI method (figures 2.6 and 2.7). The centre of mass of an ellipse is based only on its dimensions. Since ellipses are symmetrical, the similarity between each method's predictions of the centre of mass shows that transverse plane slices are reasonably symmetrical, at least in how mass is distributed. The location of the centre of mass, and how this mass is distributed directly affects moment of inertia calculations. As ellipses address these issues in a positive manner, the focus may then shift to choosing a proper density for each ellipse when estimating slice mass and moment of inertia about the centre of mass.

Moment of Inertia

While ellipses have been shown to be a good method of measuring mass and centre of mass for slices in the transverse plane, the truest test of whether ellipses can be used to represent transverse slices in the human body is whether or not they can accurately model the moment of inertia about the centre of mass. There are many ways of estimating mass, but how that mass is distributed is of key importance in moment of inertia calculations. Therefore, if the ellipses can prove to be an accurate predictor of moment of inertia, they may then be used to represent human body segments.

Moment of inertia estimates for lean tissue density ellipses showed the lowest %RMS error and best followed the shape of the MRI digitization method's slice prediction curve for the whole body when compared to the Winter and hybrid profiles. While moment of inertia calculations for the lean tissue density method proved the best results, a qualitative analysis of figure 2.9 shows that most of the error in the hybrid method's estimates take place between slices 28 and 38. This may be due to the poor estimation of mass in that region. As figure 2.5 shows, there is a dip in mass estimation below both the MRI and DPX plots. As stated before, this region contains the lungs. It is possible that a density value of $0.92 g/cm^3$ does not adequately define the true density of the region that contains the lungs. This density value is based on the average density of the whole chest. As one moves down the body, the lungs take up an increasing amount of the volume of each slice. Thus, it is quite reasonable to assume that chest slices containing lungs would have an ever-decreasing density as the area containing lungs increases. It is therefore reasonable that using a within-segment density profile similar to that suggested by Wei and Jensen (1995) would produce better results.

Both the lean tissue and hybrid density profiles show estimation errors when predicting slice moment of inertia in both the lungs and lower abdomen region. The Winter density profile, on the other hand, only shows an underestimation in the lung region. One could incorporate the Winter density profile's lower abdomen values into the hybrid model, but this would come at the expense of the hybrid model's better estimation of slice mass (Winter method's slice mass errors in that region are as high as 0.3 kg compared to half that for the hybrid model against MRI digitization and DPX measurements).

Arms

Specifically looking at arm data, low %RMS errors and high R^2 values show that uniform density ellipses generated from MRI images predict well for mass, centre of mass, and moment of inertia about the centre of mass for transverse plane slices when compared to the MRI digitization method. The error seen in the ellipses translates to, at worst, a 0.02 kg mass and a 4 mm centre of mass difference. Moment of inertia estimates are, at worst, about 20 to 30 $kg\text{-}mm^2$. Most of the error in the arms is seen at the proximal end. The proximal end of the arm is quite sensitive to position changes, such as a shoulder shrug or arm abduction. Unfortunately, the nature of the MRI machine required the subject to have his arms adducted, close to the body. It was not possible to have the subject in this position during the DPX scan, since it would have been difficult to distinguish between mass belonging to the trunk and that belonging to the arms. Though the arm abduction for the DPX scan was minimized as much as possible, the subject was not in the exact same position for both scans.

Reliability of the MRI digitization method

The analysis of variance ($\alpha = 0.05$) showed that there is no significant difference between estimates of mass, centre of mass, and moment of inertia for both the intra and inter-rater re-digitization of six transverse plane slices. The R^2 values show a high correlation between the original prediction and the repeat estimates for each variable examined. The high correlation for the inter-rater re-digitization shows the method has an insignificant level of researcher bias when distinguishing between tissues for an MRI image. Therefore, it is reasonable to state that the MRI digitization method as laid out in this paper is reliable in its ability to estimate mass, centre of mass, and moment of inertia about the centre of mass from transverse plane MRI images.

Conclusion

While ellipses produced poor estimates of the moment of inertia about the centre of mass for transverse plane slices in certain regions, the mass and centre of mass calculations suggest a promising future for ellipses. It is reasonable, through an analysis of the evidence above, that applying a more accurate density profile will produce more accurate mass estimations on a slice-to-slice basis, and thus, lower the high errors seen in the moment of inertia calculations. If this can be done, the ellipses may be stacked in order to create geometric solids that represent entire human body segments.

Future studies should study how the density changes within segments in order to create density profiles that can be applied to the ellipses. As well, these ellipses should be tested on a larger population. The method described in this study may be expensive and time consuming, thus other techniques, such as photogrammetry, may be used to generate such ellipses. Before this can be done, it is suggested that the method outlined in this study be compared to a photogrammetry method similar to one described by Jensen (1978).

Study 3
Measuring BSPs using photogrammetry as compared to MRI and DPX

Purpose

Having established in the previous study the potential for predicting inertial characteristics of transverse plane body slices using uniform density ellipses generated from MRI images, the next step was to develop a technique to generate such ellipses without the expense and time commitment of MRI digitization. An established technique for generating such ellipses is photogrammetry. The purpose of this study was to test the suitability of photogrammetry as a tool for the development of an elliptical model. Since DPX does not yield data in three dimensions, the MRI digitization method and ellipses generated from MRI images were used as an intermediary for the comparison with DPX measurements. It was hoped that uniform density ellipses generated from photogrammetry could be used to accurately estimate the inertial parameters estimated from MRI in the transverse plane.

Equipment

Digital Camera

The camera used in this experiment is the Canon PowerShot S200 Digital ELPH. The camera produces 2 mega-pixel (1600 x 1200), jpeg format, colour images. The shutter speed is automatic, between 1/1500 and 1 second depending on light intensity. The camera has a 2x optical zoom, 5.4(W) – 10.8(T) mm lens. In order to minimize distortion produced by the lens, pictures were taken at a distance from the subject, and the maximum zoom was used.

Subject

The subject used in this study was the same subject who participated in studies 1 and 2 (see studies 1 and 2 for details). Data and terminology concerning the subject in this study were handled in the same manner as outlined in the previous two studies.

Methods

The subject layed on a table in a similar manner to that for the DPX and MRI scans. Two pictures were taken of the subject. One picture was taken in the frontal plane from a distance of 3 metres, and the other was taken at 90 degrees from frontal plane, in the sagittal plane, also at a distance of 3 metres. Each picture was digitized; separating the body into 133 transverse plane slices (9 pixels apart), head to ankle. Using landmarks on the body, the two pictures were matched. The 133 slices created from the photos were then matched with those from the DPX and MRI scans.

A scale was needed in order to convert pixels to millimeters. Whole body height was used as a scale for the sagittal plane photo. The width of the table the subject was laying on was used as the scale for the frontal plane photo. It was found that the frontal

plane photo was distorted, tapering as one moved from ankle to head. To compensate for this, each slice was multiplied by a scale factor. The ratio of the width of the table at each slice to the width of the table at a spot on the photo not suffering from distortion was used as the scale factor for each slice.

Ellipses were created for each slice, and the mass of each ellipse calculated using the following equation:

$$\text{Mass} = \pi \times \text{width}/2 \times \text{height}/2 \times \text{depth} \times \text{density} \quad [1]$$

The width of the ellipse is the measured distance across the body using the frontal plane photo. Height was defined as the measured distance along the anterior-posterior axis of each slice using the sagittal plane photo. The depth of the ellipse is defined as 13.16 mm, which is the distance between slices head-to-toe as defined using the DPX scan.

Density was defined in three different ways. In the first case, a density of 1.1g/cm^3 was chosen (Siri, 1956). Lean tissue has a density of 1.1g/cm^3 and this value was chosen because a large portion of the body was defined as lean tissue in the MRI digitization process. The second case used a density profile as described by Winter (Winter, 1990). Figure 3.1 describes the density used for each section of the body.

Regions	Slices	Density (g/cm^3)
Head and Neck	1-23	1.11
Chest (with shoulders)	24-30	1.00
Chest	31-45	0.92
Abdomen	46-77	1.01
Thigh	78-110	1.05
Shank	111-133	1.09

Figure 3.1: Density profile (Winter profile) used in second method for calculating ellipse mass.

The third method used was a hybrid of the other two methods. All slices used a density value of 1.1g/cm^3 except for slices 32-45. These slice contained the lungs, and a density value of 0.92g/cm^3 was chosen based on the Winter anthropometric tables.

Centre of mass in the x-axis was calculated as half the width of the ellipse, while the centre of mass in the y-axis was calculated as half the height of the ellipse. The moment of inertia about the centre of mass for each ellipse was calculated using the following equation:

$$I = 1/4m \times [(\text{height}/2)^2 + (\text{width}/2)^2] \quad [2]$$

...where m is the mass of the ellipse. The moment of inertia about the centre of mass was calculated using the mass from the lean tissue density, the Winter density profile, and the hybrid methods.

BSPs calculated for each slice using the above method were compared to those calculated in studies 1 and 2.

Arm data was subject to the same methods as outlined above. One exception to this is that the arms use the same density value in all three profiles. Therefore, the uniform density ellipses use only one profile (as per study 2). The density value used in the arms for the uniform density ellipses is $1.11 g/cm^3$.

Mass calculations using the method above were compared against DPX slice values. The calculated inertial characteristics (mass, moment of inertia about the centre of mass) for all three ellipse methods were compared to those calculated using the MRI digitization method for each slice. Also, the ellipses developed from using photogrammetry were compared to those developed from the MRI images for each density profile. Finally, ellipse centres of mass in the x and y-axes were compared to those calculated using the MRI digitization method and MRI image generated ellipses. A summary of the %RMS errors and correlation coefficients (R^2) for each comparison is presented in appendix D.

Statistical Analysis

Slice mass estimates for each method were compared to those measured using DPX. Uniform density ellipses generated using frontal and sagittal plane photographs (lean tissue, Winter, and hybrid profiles) were compared to estimates by MRI digitization for slice mass, moment of inertia, and centre of mass (x and y-axes). As well, the uniform density photo ellipses were compared to the corresponding MRI image generated ellipses for each profile used. That is, lean tissue profile, photo ellipses were compared to lean tissue, MRI ellipses for each inertial characteristic, and so on. Percent root mean square (%RMS) values were calculated for each method comparison. As well, scatter plots were created comparing slice mass, moment of inertia, and centre of mass calculated using each profile with their DPX (for mass), MRI digitized and MRI ellipse counterparts (where possible). A regression equation was developed for these scatter plots and a correlation coefficient (R^2 value) was calculated.

Results

Whole Body

Mass

The lean tissue density profile ellipses created using photogrammetry showed a 25.5 and 25.8 %RMS error for slice mass when compared to mass measurements using the DPX scan and MRI digitization method, respectively. When compared to mass estimates yielded from the MRI digitization method, lean tissue density, photo generated ellipses produced an R^2 value of 0.8813. The regression analysis of the lean tissue profile photo ellipse mass -- DPX mass measurement comparison yielded an R^2 value of 0.9089. The mass measurement for each slice is compared in figure 3.2. When the photogrammetry ellipse slice mass estimates are compared to those of the lean tissue density MRI image generated ellipses, a 16.7 %RMS error and an R^2 value of 0.9447 is seen. Figure 3.3 shows slice mass estimations for lean tissue density ellipses using both methods.

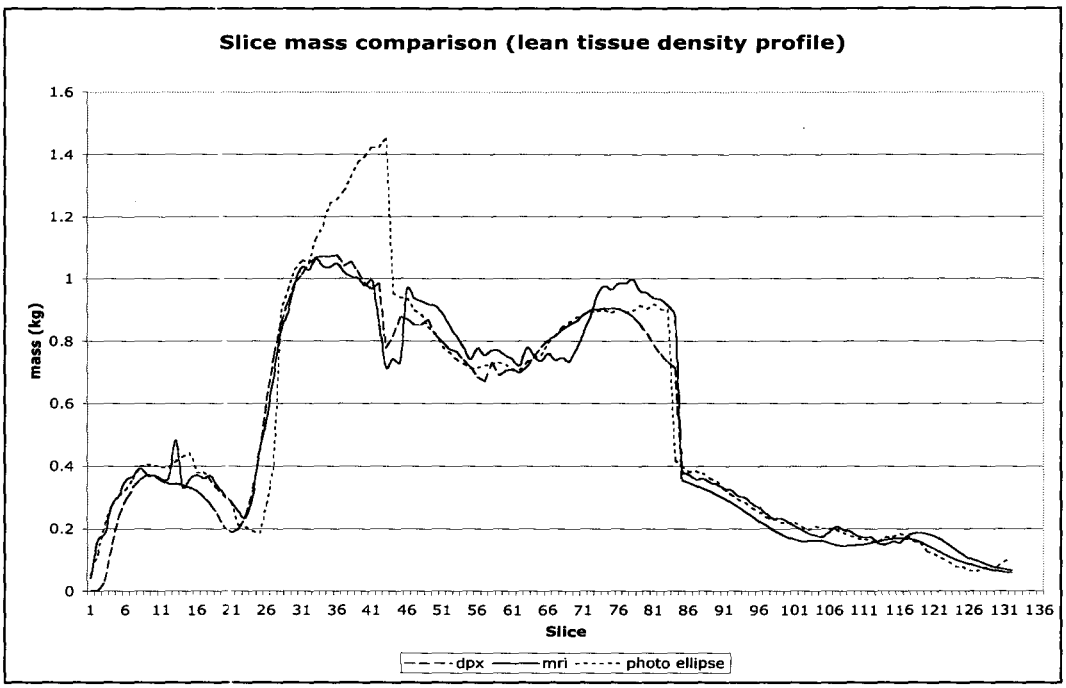

Figure 3.2: slice mass for ellipses created from photos using lean tissue density profile compared to slice mass as calculated using a DPX scan and the MRI digitization method.

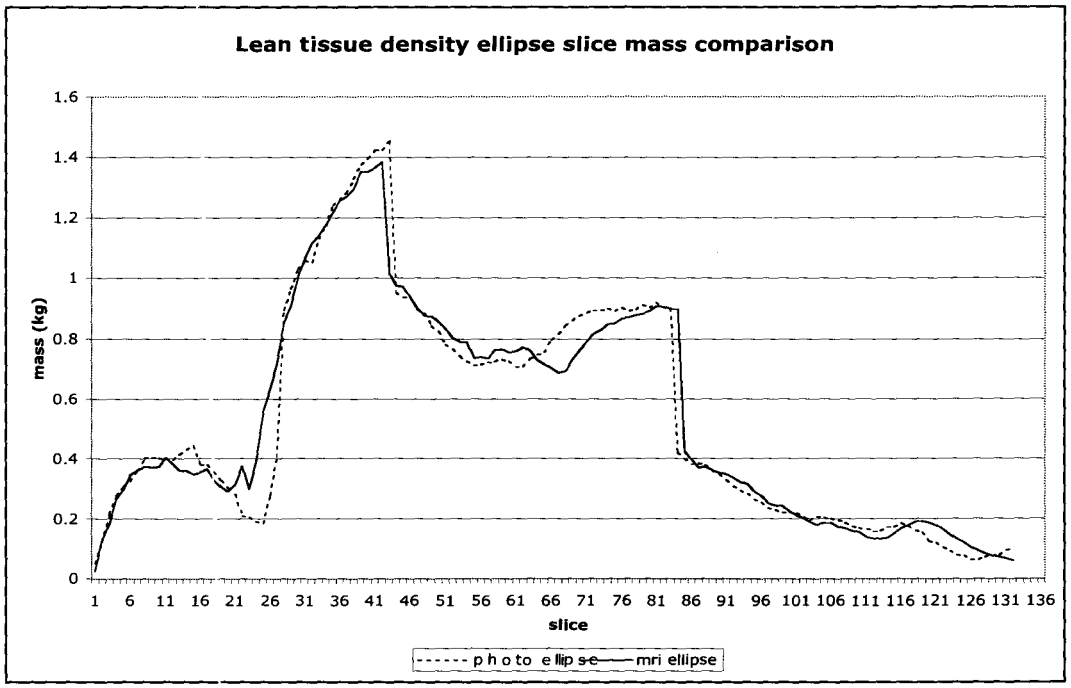

Figure 3.3: comparison of slice mass for lean tissue density ellipses created using photogrammetry and MRI methods

When the mass of the Winter density profile ellipses created using photogrammetry were compared to the DPX and MRI slice mass estimates, a 19.8 and a 20.9 %RMS error was seen, respectively. This comparison produced an R^2 value of 0.918 against DPX measurements and an R^2 value of 0.9042 against estimates using the MRI digitization method. Figure 3.4 shows the slice mass comparison for these three methods. The Winter density profile ellipses showed a 16.7 %RMS error and an R^2 value of 0.9364 when compared to the MRI ellipses (also using the Winter density profile) for slice mass. Slice mass estimations for the photogrammetry and MRI ellipses are displayed in figure 3.5.

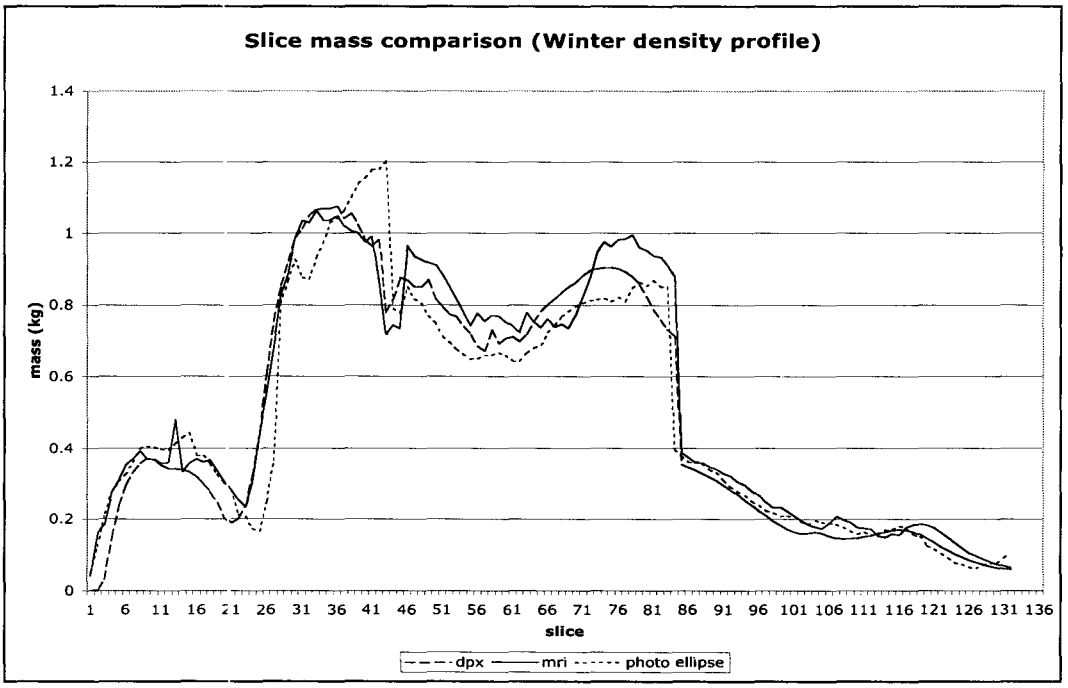

Figure 3.4: slice mass for ellipses created from photos using Winter density profile compared to slice mass as calculated using a DPX scan and the MRI digitization method.

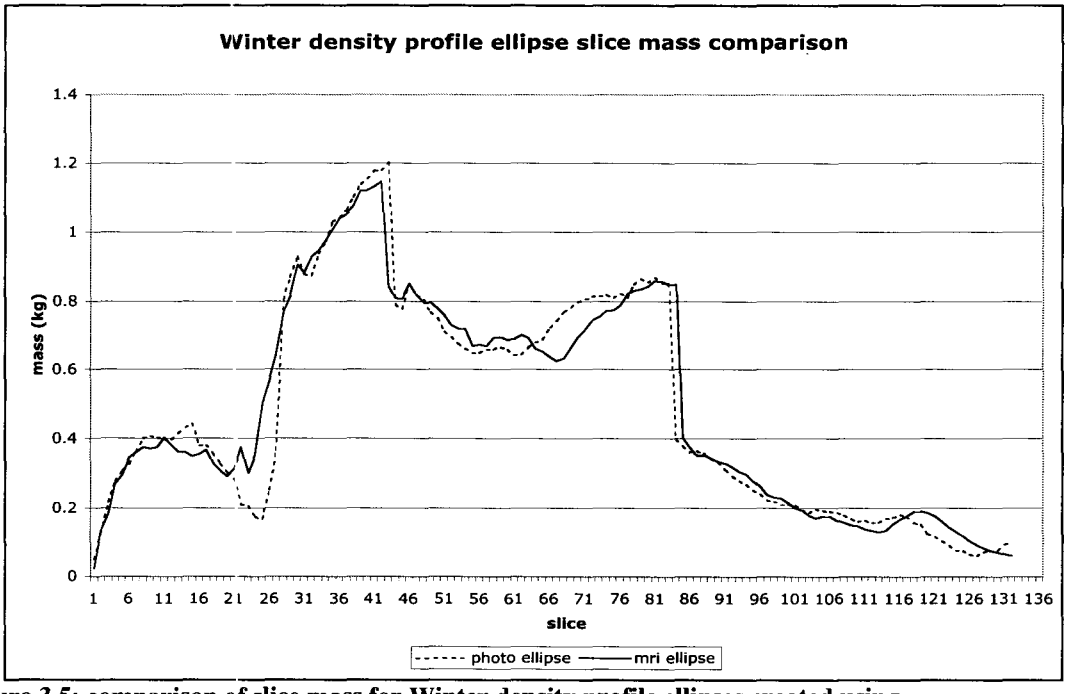

Figure 3.5: comparison of slice mass for Winter density profile ellipses created using photogrammetry and MRI methods

Photogrammetry ellipses using the hybrid density profile were compared to slice masses estimated using the DPX scan, and MRI digitization method. Figure 3.6 shows this comparison. An 18.4 %RMS error and R^2 value of 0.9345 was seen against the DPX slice mass measurement for the hybrid density photogrammetry ellipses. When compared to the slice mass estimation using the MRI digitization method, the hybrid density photogrammetry ellipses showed an 18.0 %RMS error. The same comparison showed an R^2 calculation of 0.9257 when the regression analysis was performed. The hybrid density profile photogrammetry ellipses showed a 16.8 %RMS error for slice mass when compared to the hybrid density profile MRI ellipses. The hybrid density photo ellipse – MRI ellipse comparison yielded an R^2 value of 0.9353. Figure 3.7 shows the comparison of slice mass for the hybrid density profile ellipses created using the two methods.

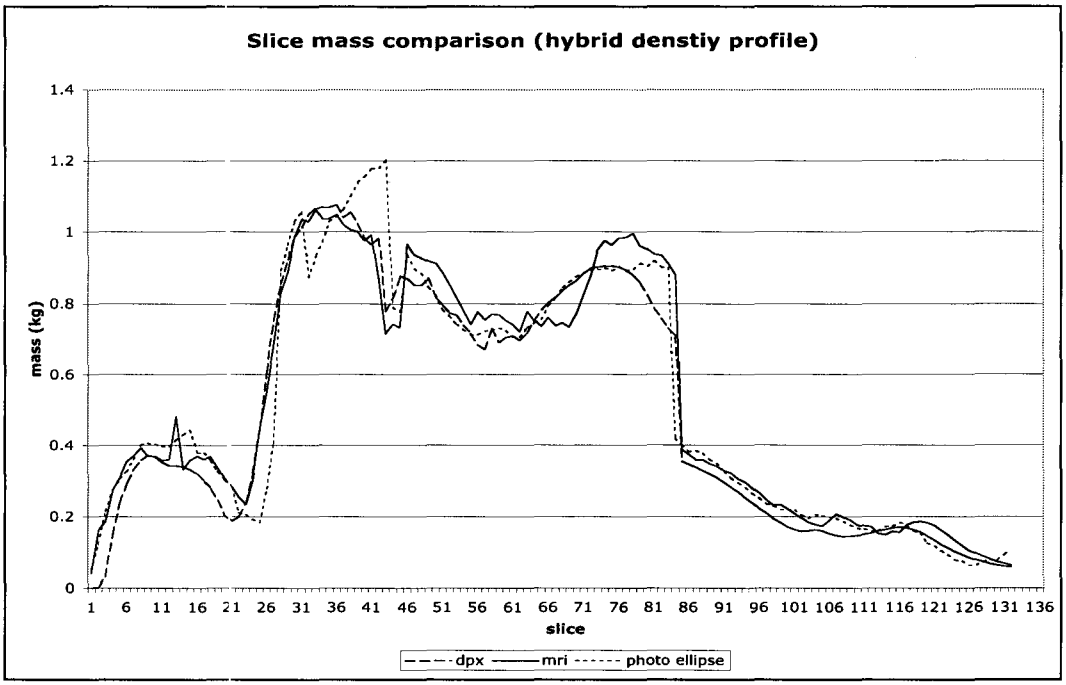

Figure 3.6: slice mass for ellipses created from photos using hybrid density profile compared to slice mass as calculated using a DPX scan and the MRI digitization method.

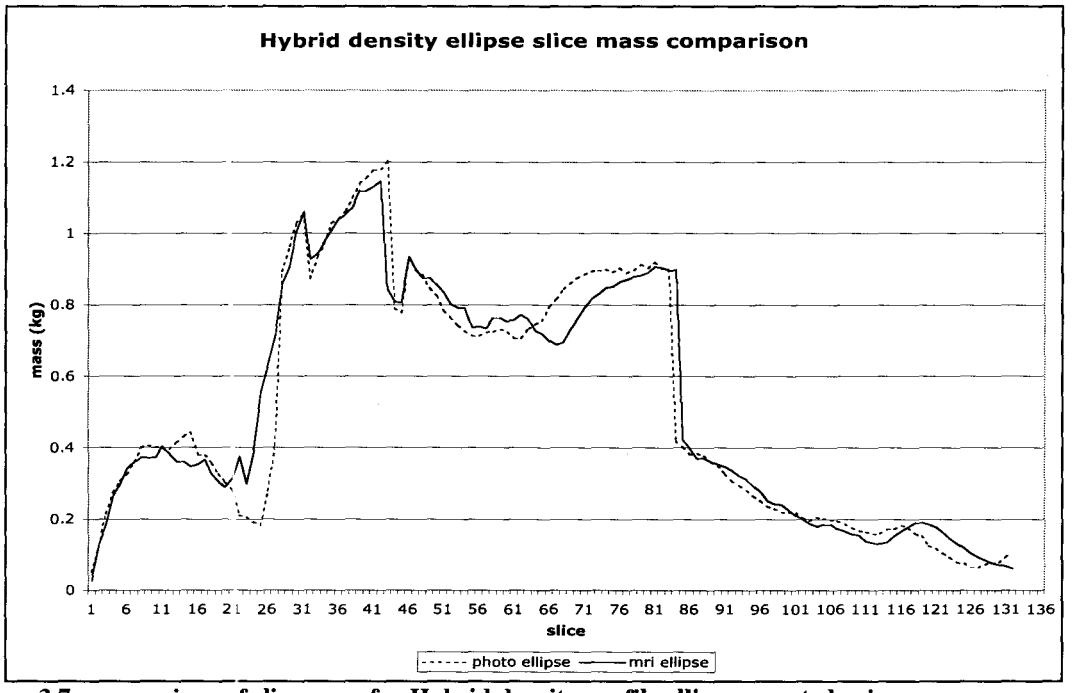

Figure 3.7: comparison of slice mass for Hybrid density profile ellipses created using photogrammetry and MRI methods

Centre of Mass

Centre of mass in the defined x-axis was calculated for each ellipse created using photogrammetry. The ellipses showed an 18.4 and 18.8 %RMS error when compared to x-axis centre of mass estimates using the MRI digitization method and MRI ellipses, respectively. Figure 3.8 compares the slice measurements for centre of mass in the x-axis for all three methods. R^2 values of 0.9014 and 0.8972 were calculated for the comparison photogrammetry generated ellipse estimates of slice centre of mass in the x-axis against slice estimates yielded from the MRI digitization method and MRI image generated ellipses, respectively.

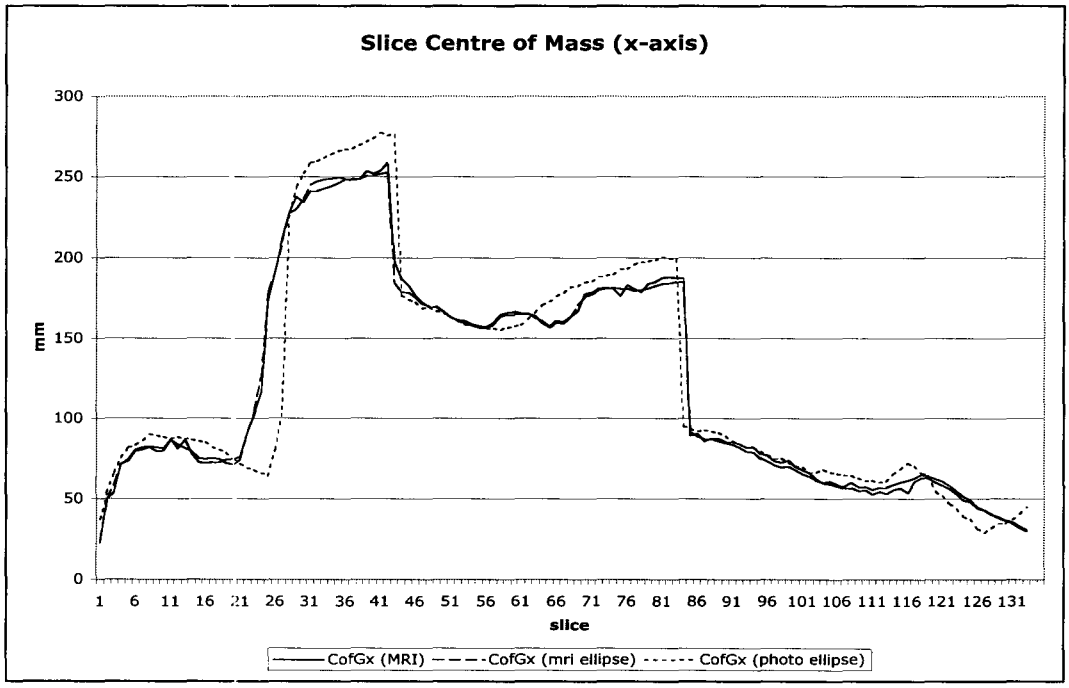

Figure 3.8: Location of the centre of mass in the x-axis. Centre of mass is the distance in the x-axis from the origin (as defined in study 2). The ellipses created using photogrammetry are compared to the MRI ellipses and the MRI digitized slices.

Centre of mass in the defined y-axis was also calculated for ellipses created using photogrammetry. When compared to y-axis centre of mass calculations for each slice using the MRI digitization method, a 10.1 %RMS error and an R^2 value of 0.9016 was seen. When the photogrammetry ellipses were compared to the MRI ellipses for centre of mass in the y-axis, an 8.0 %RMS error was calculated. The regression analysis of this comparison revealed an R^2 value of 0.9145. Centre of mass in the y-axis calculations for slices using all three methods are displayed in figure 3.9.

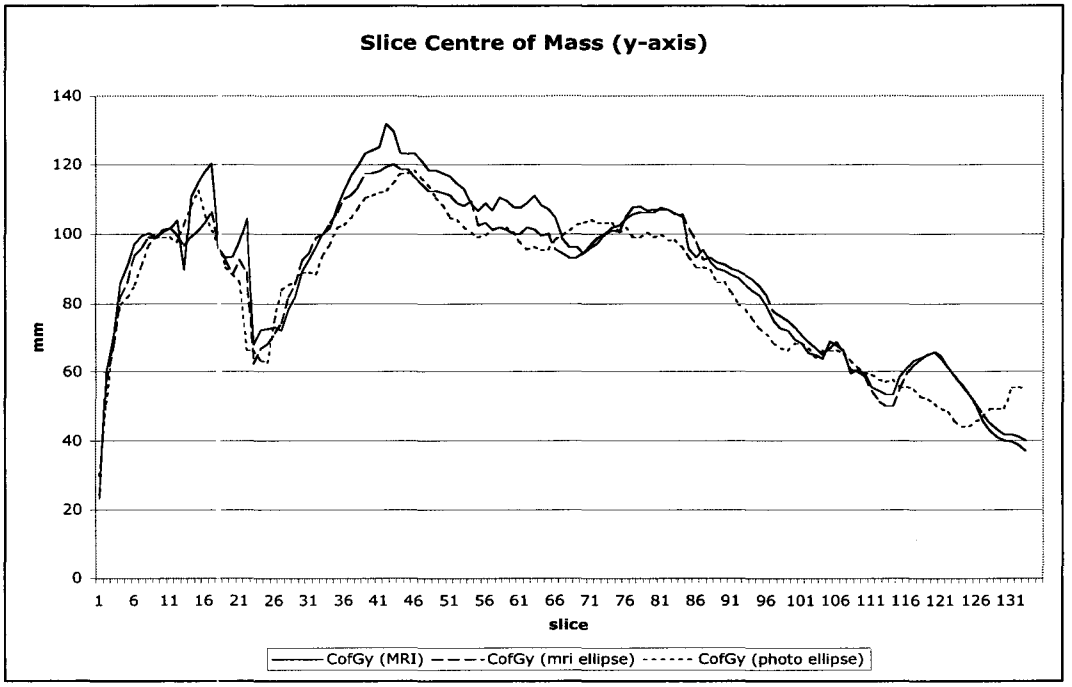

Figure 3.9: Location of the centre of mass in the y-axis. Centre of mass is the distance in the y-axis from the origin (as defined in study 2). The ellipses created using photogrammetry are compared to the MRI ellipses and the MRI digitized slices.

Moment of Inertia

The moment of inertia about the centre of mass calculations for ellipses created using photogrammetry (lean tissue density profile) were compared to slice estimates from the MRI digitization and MRI ellipse (also using lean tissue density profile) methods. The photogrammetry ellipses showed a 52.0 and 43.4 %RMS error when compared to the MRI digitization estimate and the lean tissue density MRI ellipse calculation, respectively. This comparison is displayed in figure 3.10. R^2 values of 0.8657 and 0.9236 were calculated when lean tissue density, photo generated ellipse moment of inertia estimates were compared with slice estimates using the MRI digitization method and MRI image generated ellipses, respectively.

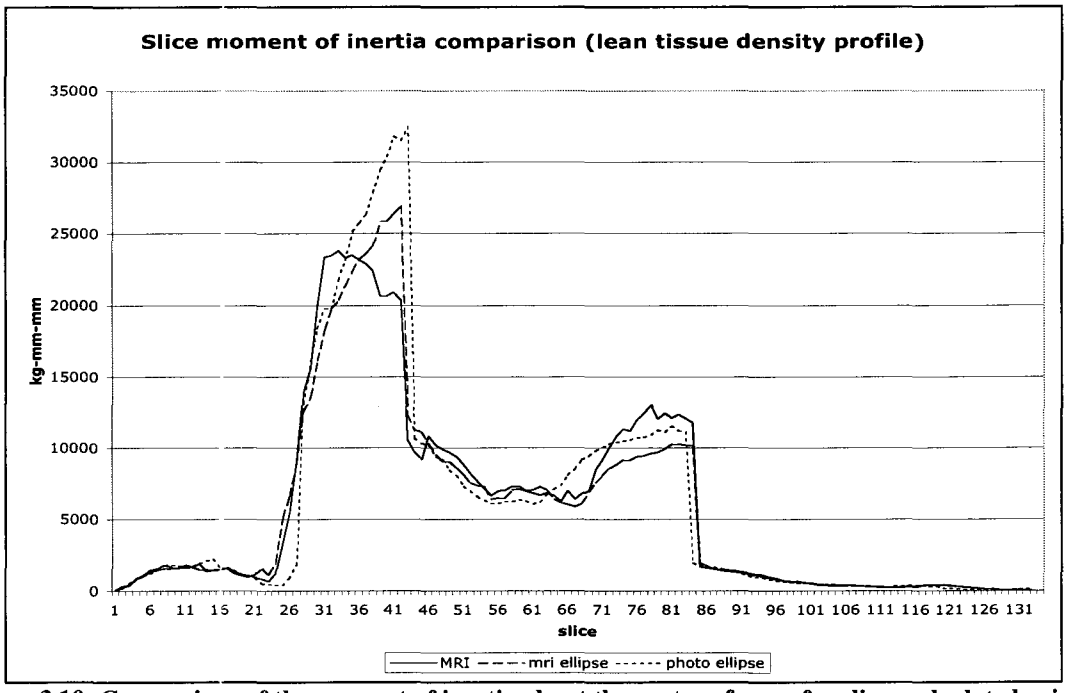

Figure 3.10: Comparison of the moment of inertia about the centre of mass for slices calculated using lean tissue density ellipses (created using photogrammetry and MRI) and the MRI digitization method.

When the Winter density profile photogrammetry ellipses were compared against MRI digitized slice and Winter density profile MRI ellipses for the measurement of moment of inertia about the centre of mass, a 42.7 and 41.6 %RMS error was seen, respectively. The regression analysis produced an R^2 value of 0.877 when photo generated ellipse estimates for slice moment of inertia were compared with those yielded using the MRI digitization method. Against the MRI image generated ellipses, Winter density photogrammetry ellipse estimates of slice moment of inertia revealed an R^2 value of 0.9182. Figure 3.11 shows the slice estimates for moment of inertia about the centre of mass for all three methods.

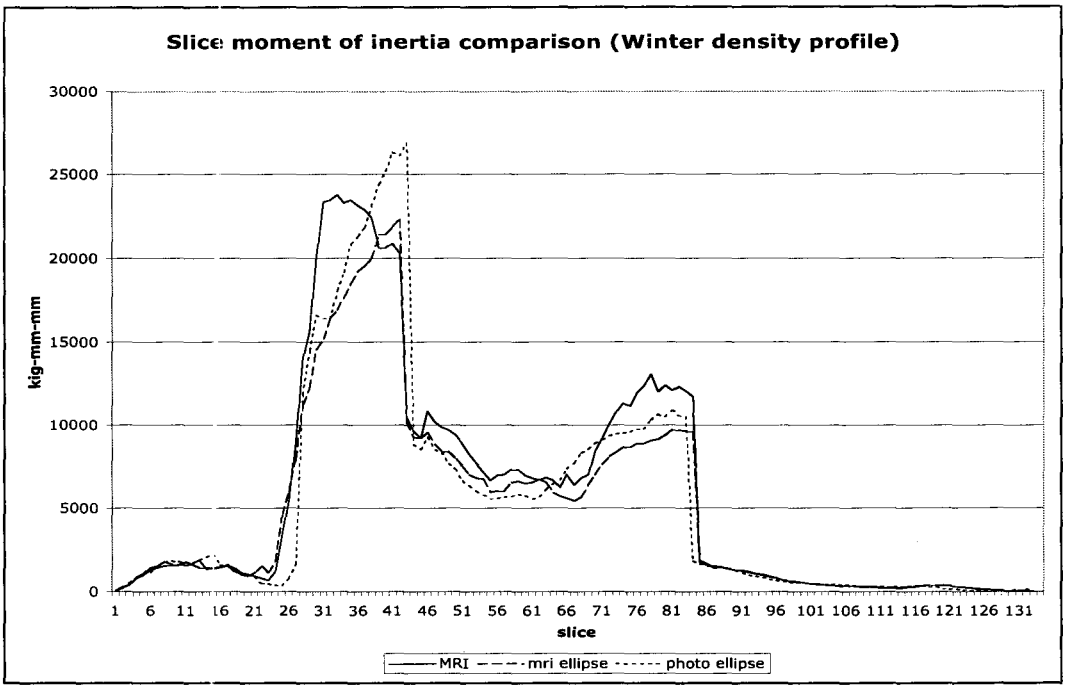

Figure 3.11: Comparison of the moment of inertia about the centre of mass for slices calculated using Winter density profile ellipses (created using photogrammetry and MRI) and the MRI digitization method.

The hybrid density profile photogrammetry ellipses were also compared to MRI slice estimates and hybrid density profile MRI ellipse measurements for moment of inertia about the centre of mass. The photogrammetry ellipses showed a 40.2 %RMS error and an R^2 value of 0.8898 when compared to the slice estimates using the MRI digitization method. A 41.3 %RMS error and an R^2 value of 0.9158 was seen when the photogrammetry ellipses were compared to the MRI ellipses (both using the hybrid density profile). Figure 3.12 compares the slice estimates for moment of inertia about the centre of mass for all three methods.

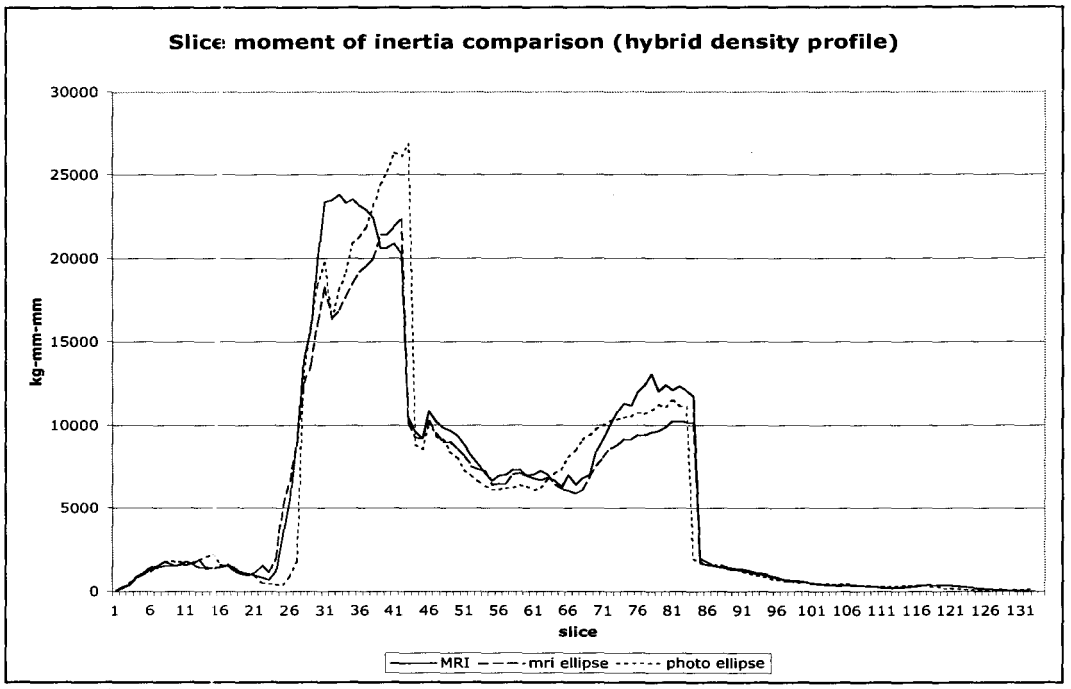

Figure 3.12: Comparison of the moment of inertia about the centre of mass for slices calculated using hybrid density profile ellipses (created using photogrammetry and MRI) and the MRI digitization method.

Arms

Mass

The masses of uniform density ellipses generated using photogrammetry were compared to slice mass estimates using the MRI digitization method. This comparison yielded a 67.4% RMS error and an R^2 value of 0.8744. When compared to DPX slice mass measurements, the photogrammetry ellipses produced an 83.5% RMS error and an R^2 value of 0.7664. Figure 3.13 compares mass data yielded from the uniform density ellipses with slice mass estimates using MRI digitization and DPX slice mass measurements. When compared to ellipses generated from MRI images, the photogrammetry generated ellipses showed a 66.9% RMS error. The regression analysis showed an R^2 calculation of 0.8036. The photogrammetry ellipse mass estimates are compared with those predicted using the MRI ellipses in figure 3.14.

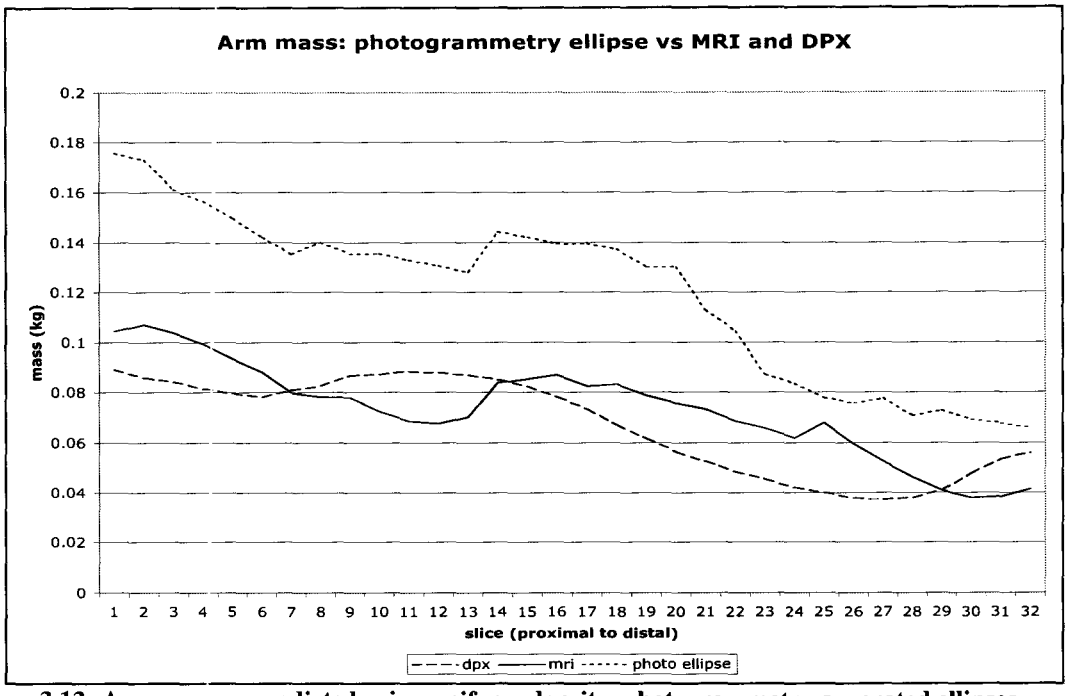

Figure 3.13: Arm mass as predicted using uniform density, photogrammetry generated ellipses compared to slice measurements using DPX and slice estimates using the MRI digitization method.

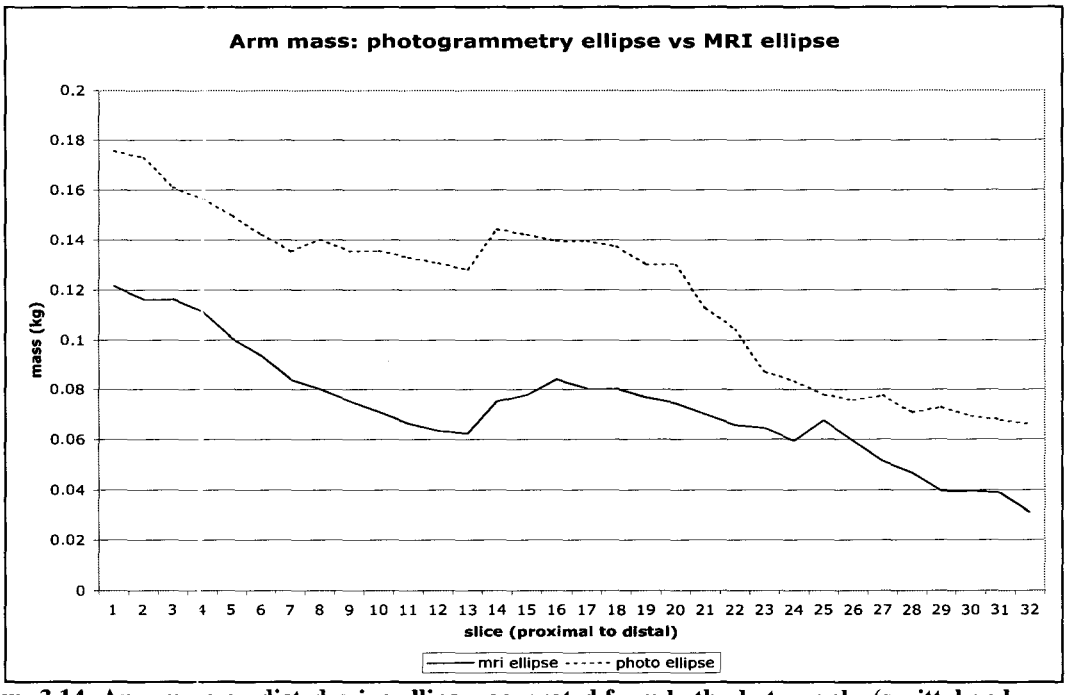

Figure 3.14: Arm mass predicted using ellipses generated from both photographs (sagittal and frontal plane) and MRI images.

Centre of Mass

Photogrammetry generated ellipses estimates of centre of mass in the x-axis showed RMS errors of 14.6% and 11.5% when compared to slice estimates using the MRI digitization method and MRI generated ellipses, respectively. Figure 3.15 displays the x-axis centre of mass prediction for arm slices using the MRI digitization method, MRI generated and photo generated ellipses. The comparison with the MRI digitization method produced an R^2 value of 0.3898, while an R^2 value of 0.5473 was calculated when photogrammetry ellipse estimates were compared to MRI ellipse predictions.

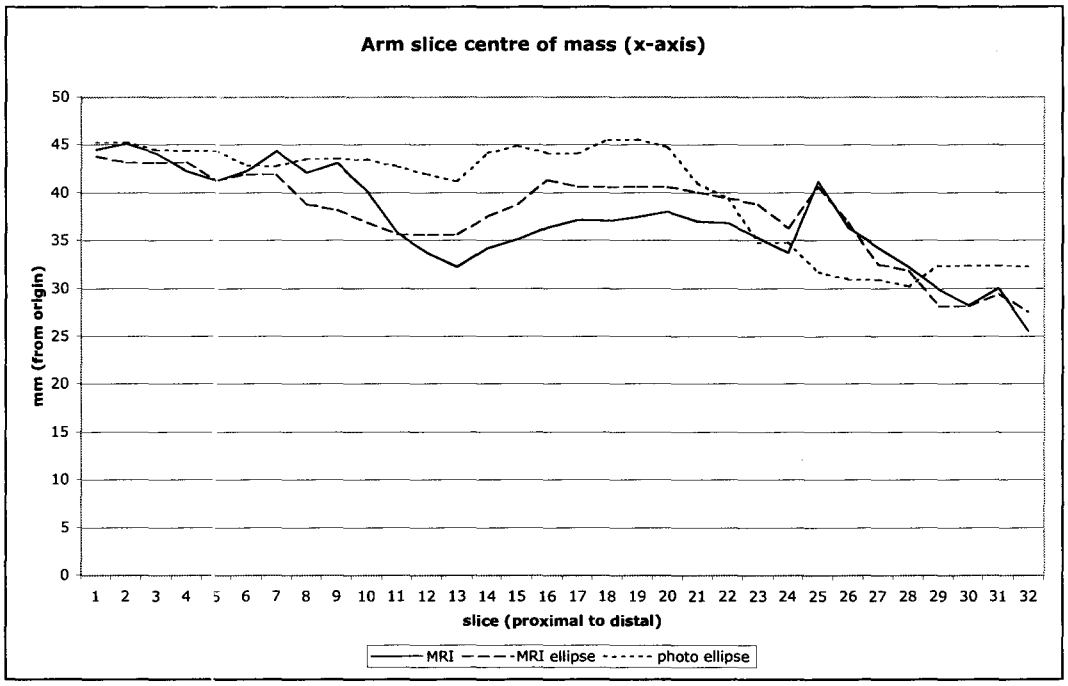

Figure 3.15: The estimate of arm slice centre of mass in the x-axis using the MRI digitization method, uniform density ellipses generated from MRI images, and uniform density ellipses generated from frontal and sagittal plane photographs.

When the photogrammetry ellipses were compared with slice estimates using the MRI digitization method, an RMS error 8.34% and an R^2 value of 0.922 was seen for centre of mass in the y-axis. When compared to MRI image generated ellipses, the photo generated ellipses saw an RMS error of 7.79% and an R^2 value of 0.8963 for centre of mass in the y-axis. Arm slice predictions for centre of mass in the y-axis using the MRI digitization method, MRI generated and photo generated ellipses are displayed in figure 3.16.

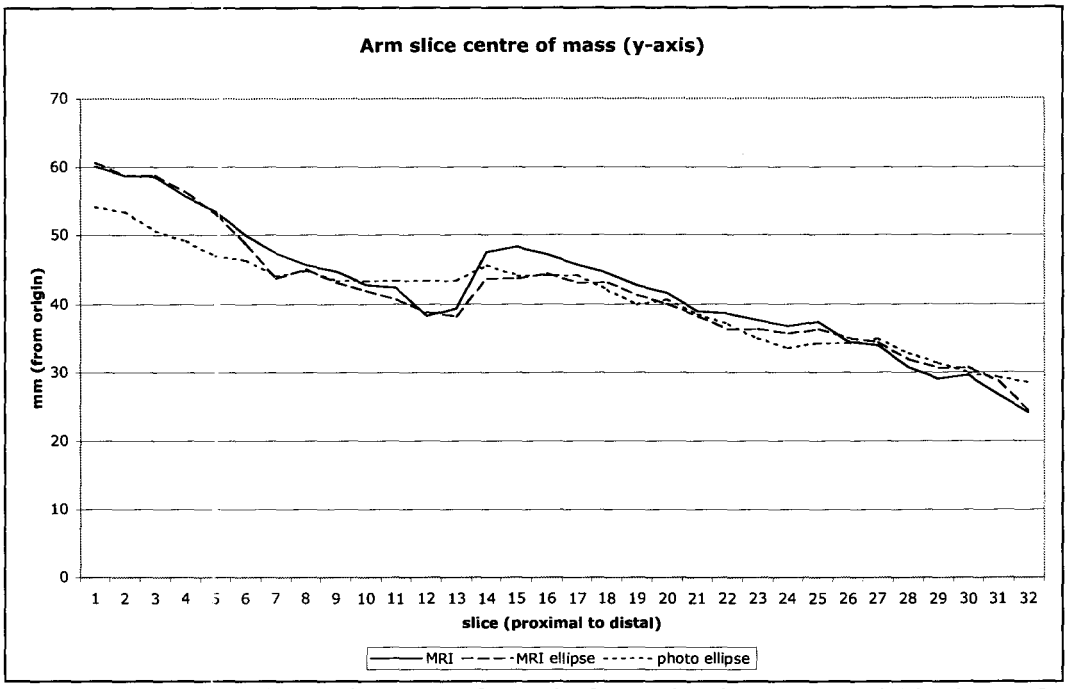

Figure 3.16: The estimate of arm slice centre of mass in the y-axis using the MRI digitization method, uniform density ellipses generated from MRI images, and uniform density ellipses generated from frontal and sagittal plane photographs.

Moment of Inertia

Moment of inertia about the centre of mass was calculated for the ellipses generated from photographs. When compared to moment of inertia slice estimates using the MRI digitization method, the photogrammetry generated ellipses showed a 183% RMS error. An R^2 value of 0.8557 was calculated from the regression analysis. When compared to slice estimates for ellipses generated from MRI images, the photogrammetry generated ellipses showed an RMS error of 176%. The regression analysis on the comparison of the two ellipse methods yielded an R^2 value of 0.7929. Figure 3.17 shows the slice estimates for moment of inertia using all three methods.

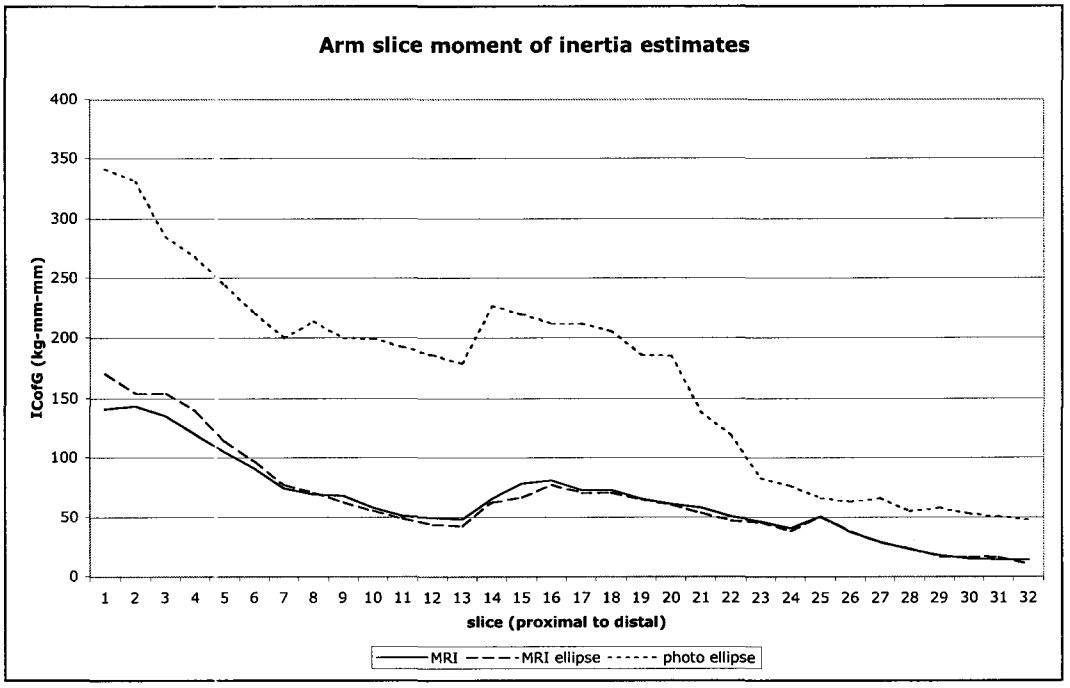

Figure 3.17: Slice moment of inertia estimates using the MRI digitization method, MRI generated and photo generated ellipses.

Discussion

Whole Body

Photo ellipse versus DPX

Uniform density, photo generated ellipse mass estimates were compared with DPX slice mass measurements for the lean tissue, Winter and hybrid density profiles. The high correlation coefficients (greater than 0.9) suggest photo ellipses have the ability to predict slice mass well. An examination of the slice mass comparison graphs (figures 3.2, 3.4, 3.6) and %RMS errors are truer tests of how well the photo ellipses predict slice mass and which profile is most accurate.

All three profiles overestimate slice mass in the head and lung regions, and underestimate in the transition zone from head/neck to trunk. The Winter profile also underestimates in the trunk. The hybrid profile, with the lowest %RMS error and the highest R^2 value, predicts slice mass best. Although the RMS error is 18.4%, excluding the lungs, this error only accounts for at worst a 0.1 kg error in slice mass, and including the lungs, 0.2 kg. As suggested in the previous study, the density of 0.92 g/cm^3 used for slices containing lungs may not be adequate for the mass prediction of those slices. The lungs take up an ever increasing proportion of transverse plane slices as one descends through the body, and the density value chosen is based on the chest as a whole. Thus, if the hybrid model could take this fact into account by changing the slice density as one

descends inferiorly through the chest, it may be able to more accurately predict slice mass.

Photo ellipse versus MRI

Estimates from ellipses generated from photos were compared to MRI digitization predictions for transverse plane slice mass, centre of mass, and moment of inertia. Each density profile used was compared with MRI digitization separately. Again the R^2 values (range 0.8657 to 0.9257) show a reasonably high correlation between the photo ellipses and MRI digitization.

Mass

Slice mass underestimations in the head/neck transition zone and abdomen, and an overestimation in the chest slices containing the lungs are seen by the photo generated ellipses for all three profiles when compared to MRI digitization estimates. Again, the hybrid profile predicts mass best, showing the lowest RMS error (18.0%) and the highest correlation coefficient (0.9257) when the three profiles are compared. The high R^2 value coupled with the hybrid profiles slice mass plot closely following the shape of the MRI slice mass estimate curve (figure 3.6) shows that the hybrid profile is useful in predicting the MRI digitization.

A close examination of the hybrid profile shows where the model is limited. Slices in the head/neck to trunk transition zone and those containing the lungs show what translates to, at worst, a 0.2 kg error, whereas the rest of the body shows an error of less than 0.1 kg for any given slice. The 0.2 kg error in the lung region may seem high, but considering that chest slices are estimated at 1.2 kg, it does not account for a great deal when compared to other regions. The most alarming error is that in the head/neck to trunk transition zone which, although only shows a 0.1 to 0.2 kg error, accounts for an error of one part in 2 (slices in this region are only 0.1 to 0.2 kg in mass). That is, these slices are being estimated at double their true mass. The transition zones are highly susceptible to position change between scans. Care in positioning the subject between scans and using a more accurate density profile through the chest will greatly increase the hybrid model's predictive ability for slice mass. To solve the positioning error, one might take the picture of the subject while he/she is positioned on the DPX or MRI table before scanning.

One concern with the elliptical representation of transverse plane slices is that uniform density ellipses may not accurately depict the mass distribution across the medial/lateral axis for chest slices. For example, the mass profile of slice 36 in appendix C shows dips where the lungs are positioned. An ellipse based on the dimensions of that slice would be flatter and would not contain the dips in the curve. Choosing the proper density for such an ellipse could produce an accurate mass estimation without following

the same mass distribution. This will not affect slice mass or centre of mass predictions, but can have adverse repercussion on slice moment of inertia estimates.

Centre of Mass

The photo ellipse slice centre of mass estimate graphs (x and y-axes) follow the MRI digitization profile (figures 3.8 and 3.9) reasonably well. This may account for the high R^2 values of 0.9014 and 0.9016 seen for x-axis and y-axis estimates, respectively. Slice centre of mass in the x-axis estimates see an RMS error of 18.4%. This translates to an error of 25 mm is the chest and as high as 150 mm (2.5 times the true estimate) in the head/neck to trunk transition zone. The y-axis sees an RMS error of 10.1%. This is at worst an estimation error of 10 mm.

Errors in y-axis centre of mass position can be explained in regions containing the spine. Ellipses put the centre of mass in the exact middle of the slice. Since the spine is of higher density than most body tissue and is positioned posterior in the body, slices containing the spine will not have a y-axis centre of mass positioned in the geometric centre of the slice. That is, one would expect to find the centre of mass slightly posterior to that predicted by the ellipse. The x-axis error suggests a discrepancy in subject position between the MRI scan and the frontal plane photograph.

Moment of Inertia

Slice moment of inertia graphs (figures 3.10-3.12) show that the photo ellipse estimates follow the profile of the MRI digitization slice predictions reasonably well. The hybrid profile, with its higher correlation coefficient (0.8898) and lower RMS error (40.2%) when compared to the lean tissue and Winter profiles, predicts best.

Initially, it would seem that an error of 40.2% would suggest the hybrid model's ability to estimate slice moment of inertia (taking the MRI digitization to be accurate) is poor. Taking into account that moment of inertia calculations are dependent on mass measures, one would anticipate that the highest errors would be seen in the regions where the model is limited in predicting mass. An examination of figure 3.12 shows this to be the case. The hybrid model does not predict moment of inertia well in the head/neck to trunk transition zone (where greater than 100% error is seen), nor does it predict well in the region containing the lungs. As well, as one moves inferiorly through the lower abdomen, the hybrid model over, then underestimates, slice mass. This translates to a similar estimation error when calculating for moment of inertia about the centre of mass for slices in that region.

Again, a better density profile will allow for more accurate slice mass estimates. Since slice moment of inertia depends on mass, this would translate into improved slice moment of inertia estimations. More accurate positioning between scans would also improve the accuracy of the hybrid model for slice moment of inertia. Chest slice

moment of inertia estimates, on the other hand, may be bound to the limitations of an ellipse in following the mass distribution of a transverse plane slice. That is, ellipses do not account for the dips that are seen in the lungs when mass is graphed in the transverse plane (Appendix C, slice 36).

Photo ellipse versus MRI image generated ellipse

Uniform density ellipses generated from sagittal and frontal plane photographs were compared to ellipses generated from MRI transverse plane images for slice mass, centre of mass, and moment of inertia about the centre of mass. Ellipses were compared with each other based on the density profile used. A regression analysis examining these estimates yielded high R^2 values (greater than 0.9) for the comparison of the two elliptical models. This, and an examination of the ellipse slice comparison graphs (figures 3.3 to 3.11) for each BSP measured, shows that there is a high correlation between the two elliptical models.

Mass

Photo ellipses using each density profile see an RMS error of 16.7% for slice mass when compared to their MRI ellipse counterparts. As well, this comparison yielded correlation coefficients (R^2) of approximately 0.94. Discrepancies in slice mass estimation for the head/neck to trunk transition zone and in the abdomen account for the majority of the error seen. This is the case for all three density profiles. The abdomen region sees an error of 0.1 kg at worst, while the error for the transition zone is much higher (0.2 to 0.3 kg). Again, the error in the transition zone is proportionally higher, accounting for a two to three times overestimation in slice mass. Accurately positioning the subject for the photographs in the same manner as for the MRI scan should eliminate the error seen between the two ellipse methods.

Centre of Mass

Comparisons between the photo and MRI generated ellipses see RMS errors of 18.8% and 8.0% for x and y-axis slice centre of mass, respectively. Figure 3.8 shows the x-axis error accounts for up to a 150 mm error in the head/neck to trunk transition zone and an error of 25 mm at worst for the rest of the body. An examination of figure 3.9 shows the RMS error translates to a maximum 10 mm discrepancy in y-axis centre of mass position.

The slice centre of mass errors are similar to the difference seen when the photo ellipses were compared to MRI digitization estimates. Such data suggests there is a scaling issue with ellipses generated from photographs. That is, the photo ellipses are based on different dimensions than the MRI image generated ellipses. Since the centre of mass for an ellipse is the geometric centre, an overestimation suggests an ellipse that is too long, while an underestimation indicates an ellipse that is too short. Figures 3.8 and

3.9 show chest and lower abdomen slices are too wide in the x-axis and too short in the y-axis. An incorrect shape may account for a mass error. It follows that a mass error, coupled with a shape error (shape differences alter the distribution of mass) can have adverse effects on the moment of inertia calculation. It is these errors that limit the slice mass and moment of inertia estimates for the photo ellipses in this study.

Moment of Inertia

Slice moment of inertia estimates show a similar profile between the photo and MRI ellipses when such slice estimates are plotted head to toe (figures 3.10 to 3.12). All three density profiles see an overestimation for slice moment of inertia in regions containing the lungs and in the lower abdomen. As well, an underestimation is seen in the head/neck to trunk transition zone. The ellipse comparisons yielded RMS errors of approximately 42% and R^2 values of 0.92. The correlation coefficients suggest similarity in the two elliptical models when estimating slice moment of inertia. Although 42% is a high level of error, it would seem that the slice moment of inertia error is due to the compounding of the slice mass error (moment of inertia calculations are dependent on mass data).

Arm

The arm is highly susceptible to position changes between scans and photographs. Thus, it is reasonable to assume that one should expect many of the problems seen in the transition zones (such as the head/neck to trunk). As stated in the methods, the only one density profile (lean tissue density) was used for the arm. For many slices, the photo ellipses correlate well with DPX, MRI and MRI generated ellipses.

Mass

When the photo ellipses are compared to DPX estimates for slice mass, an R^2 value of 0.7664 was calculated. Contrast this with the R^2 value (0.8744) calculated for the comparison of the photo ellipses with MRI digitization estimates. As was seen in study 1, the DPX arm data does not match up well with the MRI data. Since there is a higher correlation with the MRI digitization estimates, it is reasonable that the lower R^2 value coupled with the RMS error of 83.5% for the DPX comparison suggests a position change in the arm between the DPX scan and the photographs. Looking at the 67.4% RMS error for the photo ellipses compared to MRI, the high correlation and the high %RMS error imply a constant error. If one examines figure 3.13, one can see that most arm slices are out by a factor of close to 2 for slice mass.

Results similar to the MRI digitization comparison are seen when the photogrammetry ellipses are compared to the MRI image generated ellipses. This comparison yielded an R^2 value of 0.8036 and an RMS error of 66.9%. Figure 3.14 shows photo ellipses overestimating each slice mass by 0.6 kg for the first 20 slices when

compared to MRI ellipses. These results suggest that there may be a problem with the ellipse dimensions. An examination of the centre of mass data may explain the source of this constant error.

Centre of Mass

There seems to be a high correlation (R^2 values of greater than 0.9) between the photo ellipses estimation of slice centre of mass in the y-axis and that predicted using the MRI digitization method and MRI ellipses. At worst there is a 6 mm error in y-axis centre of mass position for any given arm slice.

Photo ellipse estimates of slice centre of mass in the x-axis show R^2 values of 0.3898 and 0.5473 when compared to the MRI digitization estimates and the MRI ellipse predictions, respectively. These values show little correlation with MRI digitization and MRI ellipses for photo ellipses. Root mean square errors of 14.6% and 11.5% translate into x-axis centre of mass errors as high as 10 mm when photo ellipses are compared to the MRI digitization method and MRI ellipses, respectively. The correlation coefficients, and the error data (RMS errors and figure 3.15) show that x-axis centre of mass estimates are inaccurate. As discussed earlier, the centre of mass of an ellipse is the geometric centre, and an overestimation of centre of mass implies a greater ellipse dimension. If the x-axis dimension is too large and the y-axis dimension is accurate, mass should be overestimated. As well, the distribution of mass will change with an altering of ellipse dimensions. This fact, and the dependence on mass calculations to calculate moment of inertia will ensure a high error in slice moment of inertia estimates for the photo ellipses.

Moment of Inertia

Moment of inertia estimates are dependent on mass and the distribution of mass. There is an overestimation of the x-axis dimension of many of the arm slices for the photo ellipses. As discussed above, this has consequences on both the estimate of slice mass and the distribution of such mass within a slice. We have seen that slice mass has been overestimated by the photo ellipses. Therefore one would expect a high error in slice moment of inertia estimates. This is in fact true. Photo ellipses see RMS error of 183% and 176% for slice moment of inertia when compared to predictions using the MRI digitization method and MRI ellipses, respectively.

The photo ellipses show reasonably high R^2 values of 0.8557 and 0.7929 for slice moment of inertia when compared to MRI digitization and MRI ellipse estimates, respectively. Taking into account the RMS errors, the correlation suggests a constant error. Figure 3.17 suggests such a constant error for the first 20 arm slices. This is similar to the constant error seen for arm slice mass estimates using photo ellipses. The above evidence suggests that photogrammetry generated ellipses may be used to predict slice inertial characteristics for the arm if either the x-axis overestimation is reduced or the constant error is accounted for.

Conclusion

While uniform density ellipses generated from sagittal and frontal plane photographs do not predict mass, centre of mass, and moment of inertia about the centre of mass for transverse plane body slices as well as ellipses generated from MRI images, evidence above suggests that problems with the photogrammetry method may be solved. Also, photo ellipses have the advantage over the MRI generated elliptical model is that it is less expensive and less time consuming. The ease of this technique may allow for a model specific to an individual as opposed to those based on table values.

Specifically the hybrid model seems to predict closest to the MRI digitization method (accepted as being most accurate for slice centre of mass and moment of inertia in this study). The predictive ability of the hybrid model will become more powerful with the incorporation of a more accurate density profile (especially in the chest), such as that suggested by Wei and Jensen (1995). It is possible that some of the transverse slices may not be represented well using ellipses. Other shapes may better predict the slice mass, centre of mass, and moment of inertia. It is anticipated that this will be most true for slices containing the lungs, since ellipses may not account for the how mass is distributed in the transverse plane (See appendix C, slice 36; the dips in the lungs cannot be accounted for using an ellipse).

Overall Picture

In order to calculate the inertial characteristics of the human body, one must be able to measure mass and mass distribution. It is important for those studying human movement to have such information in three dimensions. Due to constraints in technique and technology, it is not yet possible to measure all the relevant information required for accurate BSP prediction directly in an individual. That is, no single technique or piece of equipment can give enough information to directly measure BSPs in three dimensions. For example, MRI can give information of tissue position in three axes, but does not directly measure mass. DPX, on the other hand, can measure mass but not give information on its distribution in three dimensions.

Study 1 has shown, using DPX in conjunction with MRI, that mass information can be inferred using MRI. Unfortunately, MRI image generation and analysis is both expensive and time consuming. This led to the formulation of uniform density ellipses that may be used to predict inertial characteristics for transverse plane slices.

Uniform density ellipses created using MRI images proved promising in predicting the mass, centre of mass, and moment of inertia of transverse plane slices. Though the chest and lower trunk regions showed poor slice mass and moment of inertia estimates, improvements were made on these regions using different density profiles.

Next, ellipses generated from MRI images were compared with those created using photogrammetry. It was shown that a strong relationship between MRI generated ellipses and photogrammetry generated ellipses exists for calculating mass, centre of mass and moment of inertia for transverse plane slices. As well, uniform density ellipses could reasonably predict mass when compared to DPX measurements. This was especially true for photo generated ellipses using the hybrid profile. It follows that the similarity between the MRI and photo generated ellipses allows for the use of photogrammetry in order to bypass the use of MRI in creating a model to calculate the inertial characteristics of transverse plane slices, thus making the process less expensive and time consuming.

Photogrammetry generated ellipses using the hybrid density profile show the most promise in calculating the inertial characteristics of transverse plane slices. Unfortunately, this profile is still deficient in slices containing the lungs and the lower trunk. If the hybrid model can be improved, it can be used in conjunction with the photogrammetry technique to analyze transverse body slice inertial characteristics in a larger population. The next step will be to stack these ellipses to make geometric solids that allow the prediction of predict body segment parameters, and thus the inertial characteristics of the human body.

References

Braune, W. and Fischer, O. (1889). The center of gravity of the human body as related to the German infantryman. Leipzig. (ATI 138 452. Available from National Technical Information Services.)

Chandler, R.F., Clauser, J.T., McConville, H.M., Reynolds, H.M. and Young, J.W. (1975). Investigation of inertial properties of the human body. AMRL-TR-74-137, Aerospace Medical Research Laboratory, Wright-Patterson Air Force Base: Ohio.

Chandler, R.F., Snow, C.C., Young, J.W. (1978). Computation of mass distribution characteristics of children. In: Coblentz, A.M., Herron, R.E., editors. Proc Soc Photo-Optical Instrument Engineers, 166: 158-61.

Clauser, C.E., McConville, J.V. and Young, J.W. (1969). Weight, Volume and Centre of Mass of Segments of the Human Body. AMRL-TR-69-70, Aerospace Medical Research Laboratory, Aerospace Medical Division, Air Force Systems Command, Wright-Patterson Air Force Base: Ohio.

Dempster, W.T. (1995). Space requirements for the seated operator. WADC Technical Report 55-159, Aero Medical Laboratory, Wright Air Development Centre, Air Research and Development Council, Wright-Patterson Air Force Base: Ohio.

Drillis, R. and Contini, R. (1966). Body segment parameters. TR-1166-03, New York: New York University, School of Engineering and Science.

Durkin, J.L. (1998). The prediction of body segment parameters using geometric modeling and dual photon absorptiometry. Master's Thesis. McMaster University. Hamilton, Ontario, Canada.

Durkin, J.L., Dowling, J.J. (1998). DXA software. McMaster University. Hamilton, Ontario, Canada.

Durkin, J.L. (2002). The measurement of body segment inertial parameters using dual energy X-ray absorptiometry. Journal of Biomechanics, 35: 1575-1580.

Friedman, B.R., Jones, J.P., Chaves-Munoz, G., Salmon, A.P., Merrit, C.R.B. (1989). Principles of MRI, Toronto: McGraw-Hill.

Hanavan, E.P. (1964). A mathematical model of the human body. AMRL-TR-64-102, Aerospace Medical Research Laboratories, Wright-Patterson Air Force Base: Ohio.

Harless, E. (1860). The static moments of the component masses of the human body. Trans.Of the Math-Phys., Royal Bavarian Acad. Of Sci., 8(1): 69-96. Unpublished English Translation FTD-TT-61-295, Wright-Patterson Air Force Base: Ohio.

Hinrichs, R.N. (1985). Regression equations to predict segmental moments of inertia from anthropometric measurements: and extension of the data of Chandler, et al. (1975). Journal of Biomechanics, 18(8): 621-624.

Hopkins, J. (2002). The Prediction of Body Segment Parameters Using A Proposed Elliptical Model. Undergraduate Thesis. McMaster University, Hamilton, Ontario, Canada.

Huang, H.K., Wu, S.C. (1976). The evaluation of mass densities of the human body in vivo from CT scans. Journal of Biomechanics, 6: 337-43.

Huang, H.K. (1983). Evaluation of cross-sectional geometry and mass density distributions of humans and laboratory animals using computerized tomography. Journal of Biomechanics, 16(10): 821-832.

Jensen, R.K. (1978). Estimation of the biomechanical properties of three body types using a photogrammetric method. Journal of Biomechanics, 11: 349-358.

Jensen, R.K. (1989). Changes in segment inertia proportions between four and twenty years. Journal of Biomechanics, 22: 529-536.

Jensen, R.K., Abraham C. (1990). Assumed segment densities for the elderly and the effect of changes in body shape. In: Richards, C.L., editor. Human Locomotion VI. Quebec: Canadian Society for Biomechanics, 117-118.

Jensen, R.K., MacDonald K. (1991). A modeling approach to growth curves for body segments during pregnancy [abstract]. Abstracts, Canadian Association of Sports Sciences Meeting, October 1991, Kingston, Ontario. Kingston: Canadian Association of Sports Sciences.

Jensen, R.K., Fletcher P. (1994). Distribution of mass to the segments of elderly males and females. Journal of Biomechanics, 27: 89-96.

Martin, P.E., Mungiole, M., Marzke, M.W. and Longhill, J.M. (1989). The use of magnetic resonance imaging for measuring segment inertial properties. Journal of Biomechanics, 22(4): 367-376.

Mungiole, M., Martin, P.E. (1990). Estimating segment inertial properties: Comparison of magnetic resonance imaging with existing methods. Journal of Biomechanics, 23 (10): 1039-1046.

Pearsall, D.J., Livingston, L. (1992). Center of mass of trunk segments relative to the Spine as determined by computed tomography [abstract]. In: Draganich L., Wells, R., Bechtold, J., editors. Abstracts, 2nd North American Congress on Biomechanics, Chicago: 77-78.

Pearsall, D.J, and Reid, J.G. (1994). The study of human body segment parameters in biomechanics. Sports Medicine, 18(2): 126-140.

Pearsall, D.J., Reid, J.G., and Livingston, L.A. (1996). Segmental inertial parameters of the human trunk as determined from computed tomography. Annals of Biomedical Engineering, 24: 198-210.

Plagenhoef, S. (1983). Anatomical data for analyzing human motion. Research Quarterly for Exercise and Sport, 54(2): 169-178.

Siri, W.E. (1956). Gross composition of the body. In Advances in Biological and Medical Physics, IV, J.H. Lawrence and C.A. Tobias (Eds.). New York: Academic Press.

Spitzer, V.M., and Whitlock, D.G. (1998). Atlas of the Visible Human Male. National Library of Medicine. Jones and Bartlett Publishers, Sudbury, Massachusetts.

Spivak, C.D. (1915). Methods of weighing parts of the living human body. JAMA, 65: 1707-8.

Webber, C.E. (1995). Dual photon transmission measurements of bone and body composition during growth. In: Blimkie, C.J.R. and Bar-Or, O. New Horizons in Pediatric Exercise Science. Champaign, IL: Human Kinetics Publishers, pp. 57-76.

Wei, C. and Jensen, R.K. (1995). The application of segment axial density profiles to a human body inertia model. Journal of Biomechanics, 28 (1): 103-108.

Wild, T. (1954). Simplified volume measurement with the polar planimeter. Surveying Mapping, 14: 218-222.

Winter, D.A. (1990). Biomechanics and Motor Control of Human Movement, second Ed. New York: John Wiley and Sons, Inc., pp. 51-64.

Zatsiorsky, V. and Seluyanov, V. (1983). The mass and inertia characteristics of the main segments of the human body. In: Matsui, H., Kobayashi, K. (Eds). Biomechanics VII-B (pp. 1152-1159). Champaign, IL: Human Kinetics Publishers.

Zatsiorsky, V., Seluyanov, V. (1985). Estimation of the mass and inertia characteristics of the human body by means of the best predictive regression equations. In: Winters, D.A., Norman, R.W., Wells, R.P., et al., editors. Biomechanics IX-B. Champaign: Human Kinetics, 233-239.

Zatsiorsky, V., Seluyanov V., Chugunova, L. (1990). In Vivo body segment inertial parameters determination using a gamma-scanner method. (pp. 186-201).

Zheng, Z., Zheng, X., Wang, Y., Wu, Y., Chen, W. (1990). A new method to determine inertial parameters of the segments relative to the human body [abstract]. Beijing: Asian Games Scientific Congress, 1990.

Zook, D.E. (1932). The physical growth of boys. American Journal Disabled Children, 43: 1347-432.

Appendix A

Study nomenclature - definition of axes

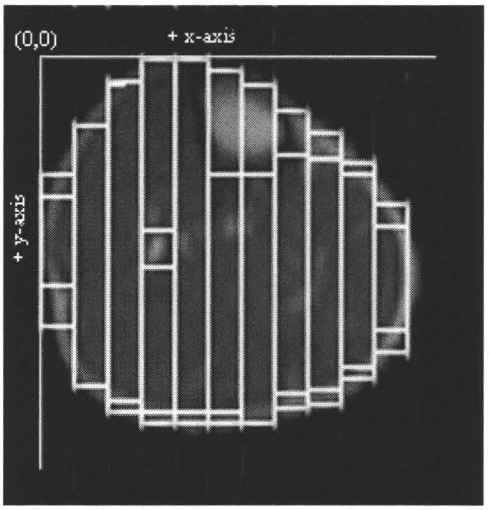

defined axes for transverse plane slices

Axis		**anatomical term**	**DPX and MRI scans**	
x	=	medial/lateral	=	columns
y	=	anterior/posterior		
z	=	inferior/superior	=	scan lines

x-y plane = transverse plane
x-z plane = frontal plane
y-z plane = sagittal plane

$I_{x\text{-}x} = I_{sag}$
$I_{y\text{-}y} = I_{front}$
$I_{z\text{-}z} = I_{trans}$

measured from DPX	**may be estimated from MRI**
m	CofGy
CofGx	I_{sag}
CofGz	I_{trans}
I_{front}	

Appendix B

Transverse plane slice mass estimation from DPX and MRI

Figure 1: Diagram of the DPX measurement of slice mass

Figure 2: Diagram of the MRI digitization method for transverse slice mass estimation

Figure 1

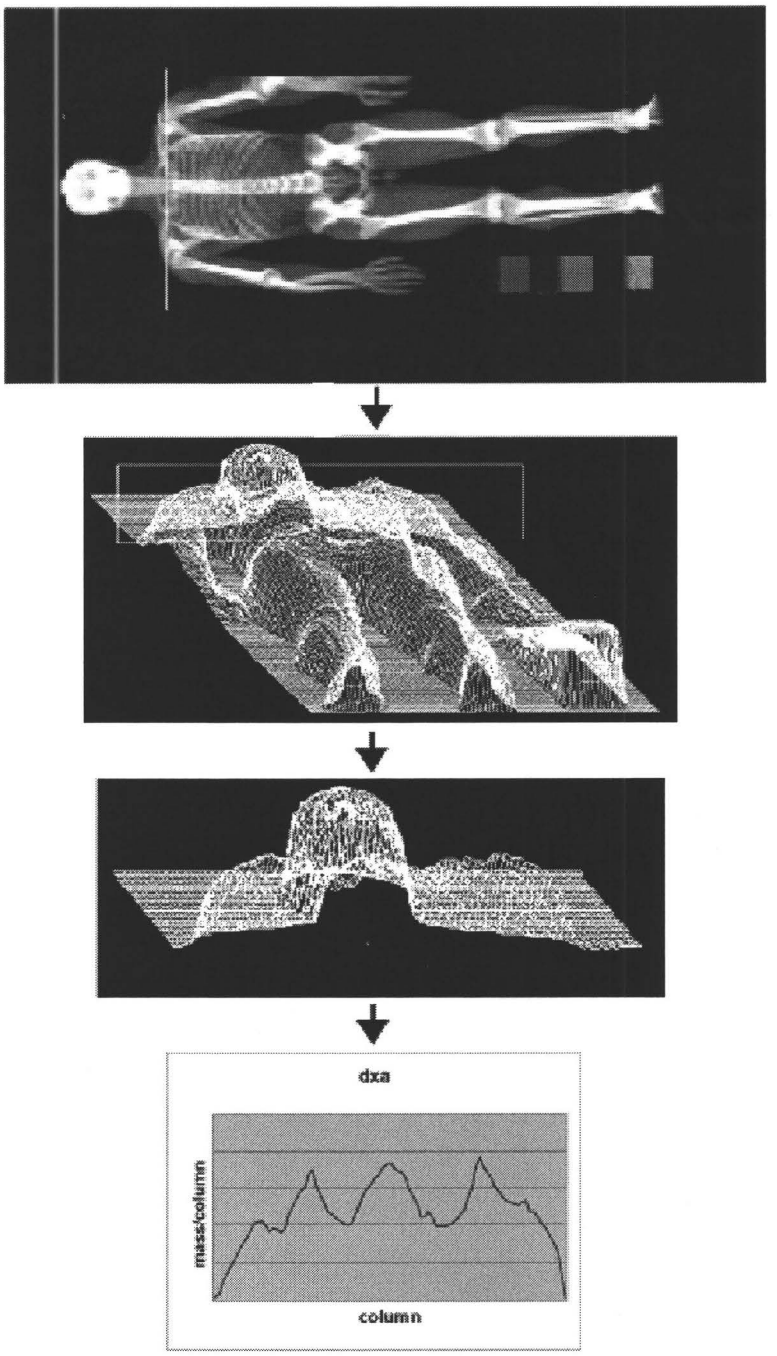

Figure 2

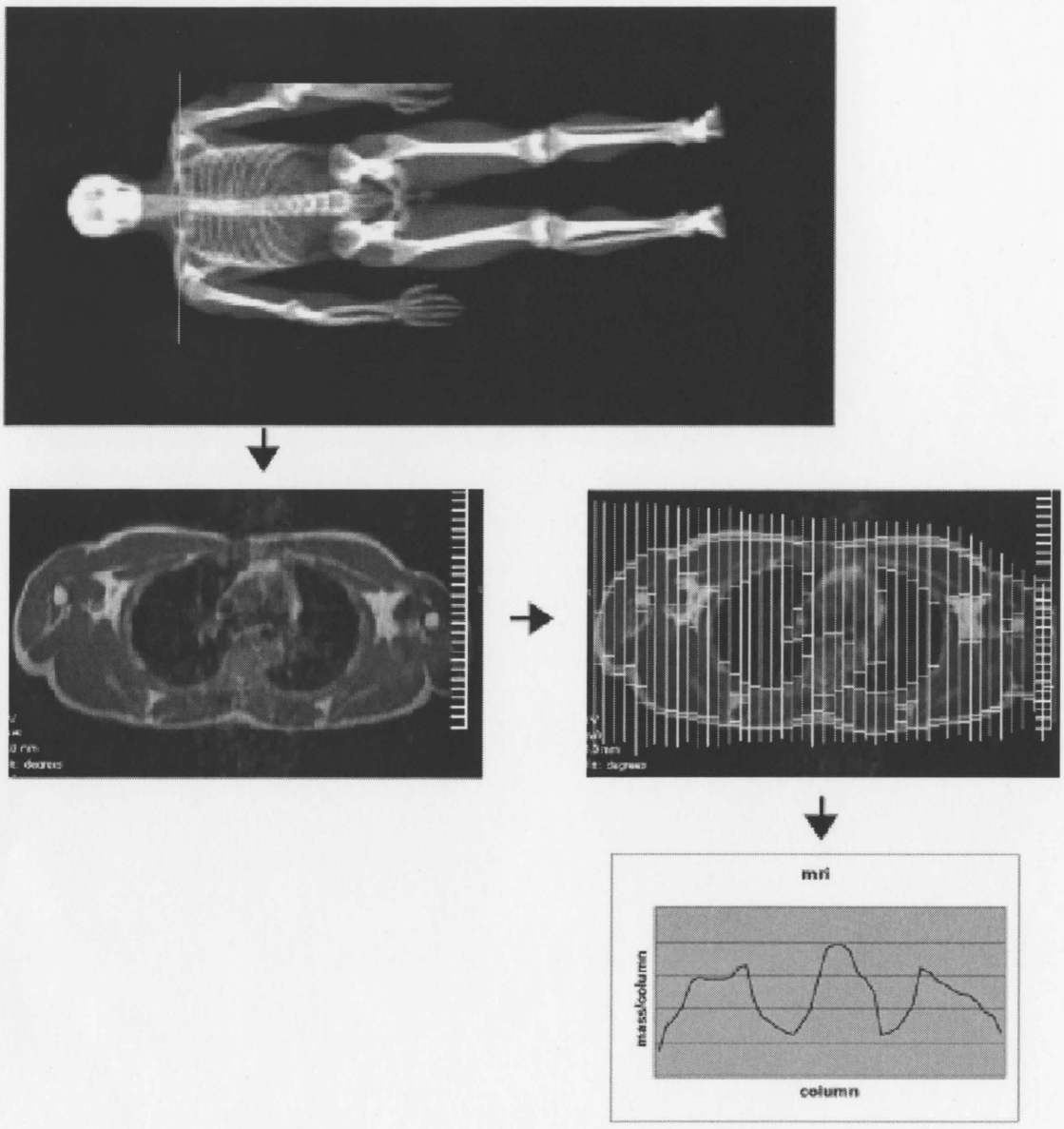

Appendix C

Comparison of mass distribution along the medial/lateral axis for transverse plane slices as measured using DPX and estimated from MRI digitization.

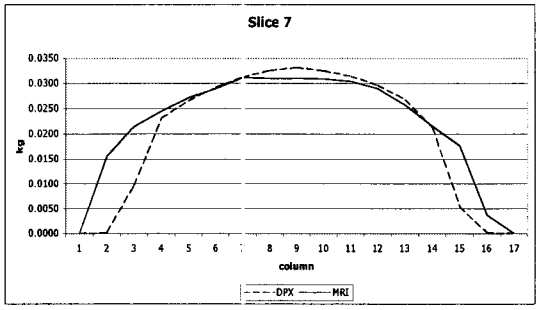
Slice 7
kg
column
DPX
MRI

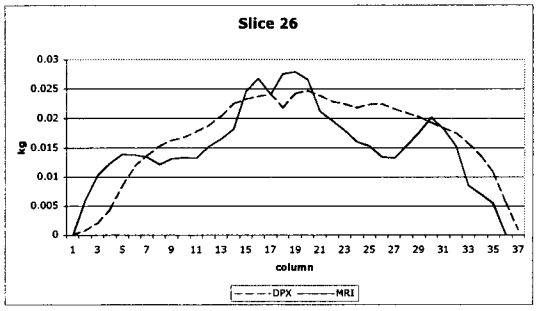
Slice 26
kg
column
DPX
MRI

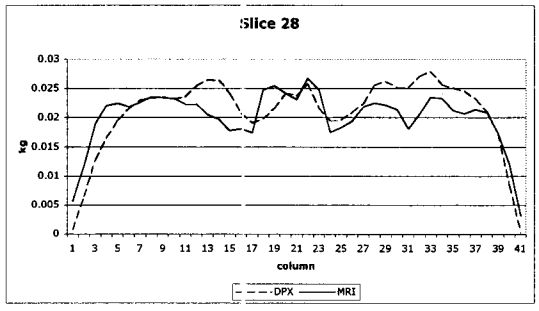
Slice 28
kg
column
DPX
MRI

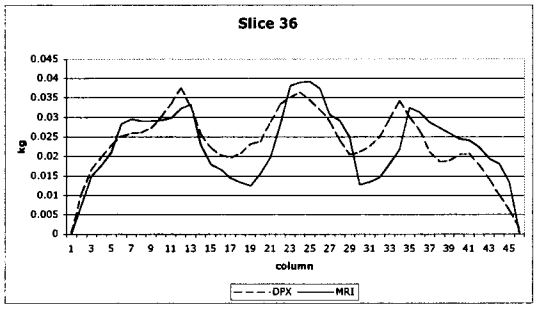
Slice 36
kg
column
DPX
MRI

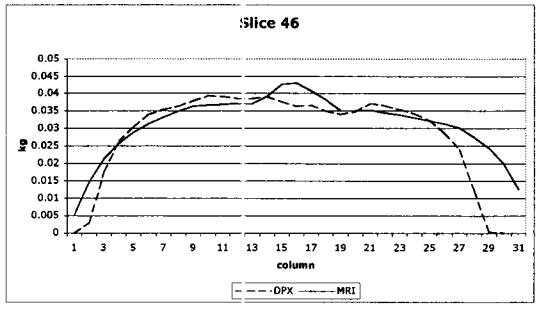
Slice 46
kg
column
DPX
MRI

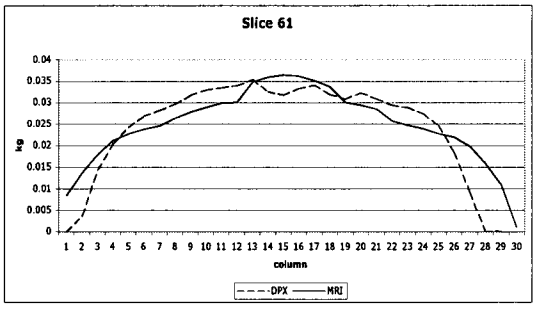
Slice 61
kg
column
DPX
MRI

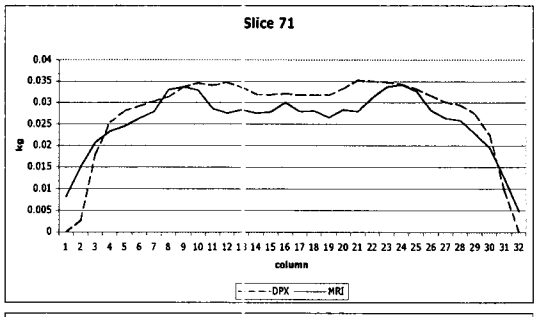
Slice 71
kg
column
DPX
MRI

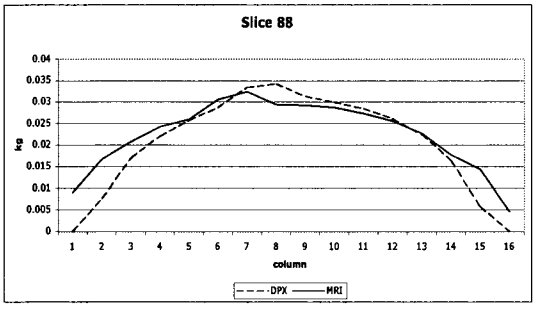
Slice 88
kg
column
DPX
MRI

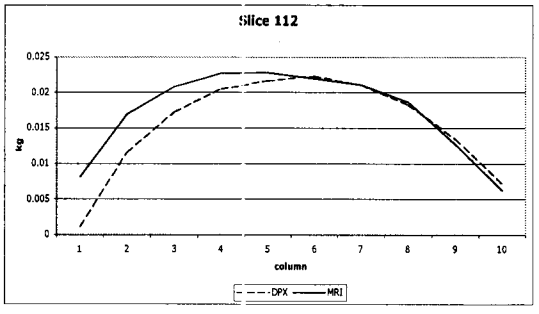
Slice 112
kg
column
DPX
MRI

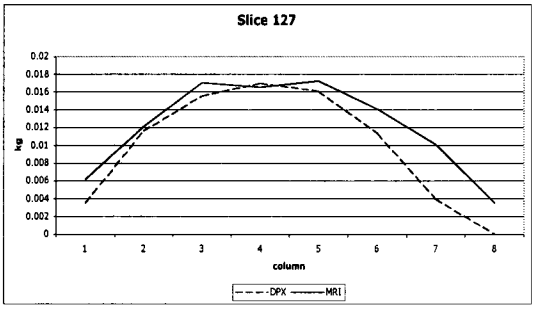
Slice 127
kg
column
DPX
MRI

Appendix D

Statistical comparison of methods (%RMS error and R^2)

	Mass		ICofG	
Whole Body	**%RMS**	**R^2**	**%RMS**	**R^2**
MRI vs DPX	12.5	0.9707		
MRI ellipse vs MRI				
Lean	18.7	0.9293	26.8	0.9529
Winter	16.0	0.9553	36.3	0.9634
Hybrid	10.8	0.9721	29.6	0.9701
MRI ellipse vs DPX				
Lean	18.4	0.9448		
Winter	15.5	0.9546		
Hybrid	13.1	0.9664		
Photo ellipse vs MRI				
Lean	25.8	0.8813	52.0	0.8657
Winter	20.9	0.9042	42.7	0.8770
Hybrid	18.0	0.9257	40.2	0.8898
Photo ellipse vs DPX				
Lean	25.5	0.9089		
Winter	19.8	0.9180		
Hybrid	18.4	0.9345		
Photo ellipse vs MRI ellipse				
Lean	16.7	0.9447	43.4	0.9236
Winter	16.7	0.9364	41.6	0.9182
Hybrid	16.8	0.9353	41.3	0.9158
Arm				
MRI vs DPX	23.5	0.4975		
MRI ellipse vs DPX	28.1	0.4212		
MRI ellipse vs MRI	8.34	0.9485	12.96	0.9787
Photo ellipse vs DPX	83.5	0.7664		
Photo ellipse vs MRI	67.4	0.8744	183	0.8557
Photo ellipse vs MRI ellipse	66.9	0.8036	176	0.7929

	CofGx		CofGy	
Whole Body	**%RMS**	**R^2**	**%RMS**	**R^2**
MRI ellipse vs MRI	2.49	0.9981	6.96	0.9724
Photo ellipse vs MRI	18.4	0.9014	10.1	0.9016
Photo ellipse vs MRI ellipse	18.8	0.8972	8.00	0.9145
Arm				
MRI ellipse vs MRI	6.91	0.7549	4.19	0.9716
Photo ellipse vs MRI	14.6	0.3898	8.34	0.9220
Photo ellipse vs MRI ellipse	11.5	0.5473	7.79	0.8963